INVESTIGATION OF THE PLASMA CHARACTERISTICS BY VARYING THE PRESSURE AND GAS TEMPERATURE INSIDE THE PECVD CHAMBER.

A DISSERTATION

SUBMITTED IN PARTIAL FULFILLMENT OF THE REQUIREMENTS
FOR THE AWARD OF DEGREE
OF

MASTER OF TECHNOLOGY

IN

NANOSCIENCE AND TECHNOLOGY

Submitted By

SAGAR KHANNA

(Roll No. 2K16/NST/06)

Under the supervision of

PROF. (DR.) SURESH C. SHARMA

DEPARTMENT OF APPLIED PHYSICS

Delhi Technological University

(Formerly Delhi College of Engineering)

Bawana Road, Delhi-110042

JUNE, 2018

DELHI TECHNOLOGICAL UNIVERSITY

(Formerly Delhi College of Engineering)

Bawana Road, Delhi-110042

CANDIDATE'S DECLARATION

I, Sagar Khanna, Roll No. 2K16/NST/06 of M.Tech. Nanoscience and Technology, hereby declare that the project Dissertation titled **"Investigation of the plasma characteristics by varying the pressure and gas temperature inside the PECVD chamber"** which is submitted by me to the Department of Applied Physics, Delhi Technological University, Delhi in partial fulfillment of the requirement for the award of the degree of Master of technology, is original and not copied from any source without proper citation. This work has not been used for the award of any Degree, Diploma Associate ship, Fellowship or other similar title or recognition.

Place, Delhi, INDIA **Sagar Khanna**

Date:

DELHI TECHNOLOGICAL UNIVERSITY

(Formerly Delhi College of Engineering)

Bawana Road, Delhi-110042

CERTIFICATE

I hereby certify that the Project Dissertation titled **"Investigation of the plasma characteristics by varying the pressure and gas temperature inside the PECVD chamber"** by Sagar Khanna, Roll No. 2K16/NST/06, Department of Applied Physics, Delhi in partial fulfillment of the requirement for the award of the degree of Master of Technology, is a record of the project work carried out by the student under my supervision. To the best of my knowledge, this work has not been submitted in parts or full for any Degree or Diploma to this University or elsewhere.

Place, Delhi, India
Date:

Prof. (Dr.) Suresh C. Sharma
HOD, Department of Applied Physics
Delhi Technological University
Delhi, INDIA

ACKNOWLEDGEMENT

I wish to express my deep sense of gratitude and veneration to my supervisor, **Prof. (Dr.) Suresh C. Sharma**, Head of Department, Department of Applied Physics, Delhi Technological University, Delhi, for his perpetual encouragement, constant guidance, valuable suggestions and continued motivation, which has enabled me to complete this work.

I am also grateful to all the faculty members for their constant guidance and facilities they provided to carry out my work. I would like to convey my special thanks to **Mr. Ravi Gupta and Ms. Neha Gupta** and all fellow scholars for their constant support and guidance.

I would like to acknowledge my dear friends **Manish Kumar, Astha Srivastava, Saumya Tripathi and Anurag** for being with me during my research work. We shared the same story and worked hard together. This experience would not have been fun without them.

Finally, I would like to thank **my family,** without whom-over the years-none of this would have been possible. They have always been there for me and I am thankful for everything they have helped me achieve.

Sagar Khanna
M.Tech (NST), DTU
Roll NO. 2K16/NST/06

Abstract

INVESTIGATION OF THE PLASMA CHARACTERISTICS BY VARYING THE PRESSURE AND GAS TEMPERATURE INSIDE THE PECVD CHAMBER.

SAGAR KHANNA

DEPARTMENT OF APPLIED PHYSICS

DELHI TECHNOLOGICAL UNIVERSITY

SUPERVISOR: PROF. SURESH C. SHARMA

The following report demonstrates the renowned technique of growing carbon nanostructures, which is plasma enhanced chemical vapour deposition. There exist many techniques like thermal-chemical vapour deposition, physical vapour deposition, laser ablation, sol-gel, sputtering, ball-milling, etc for the growth and manufacture of carbon nanostructures. Chemical vapour deposition or CVD in short, is a strategy for the creation of thin layers of polymeric materials that has viably beaten a portion of the issues went up against by wet synthetic fabrication and other affidavit strategies. There are numerous hybrid techniques that emerge from chemical vapor deposition and are consistently developing so as to enhance and alter the nature of the manufactured thin films. Among them, plasma enhanced substance vapor deposition or to put it plainly, PECVD, is a strategy that can broaden the relevance of the system for different predecessors, responsive natural and inorganic materials and additionally non-receptive or dormant materials. Moreover, by this method, one can grow carbon nanoparticles, nano-films, nano-rods and nanowires with great ease. Using COMSOL Multi-physics simulation software, we have simulated the production of plasma in a chamber that was excited with signal of RF frequency of 13.56 MHz using inductive coupling. The gases used are argon, acetylene and hydrogen. The analysis of various characteristics of plasma were done at different pressures and temperatures. PECVD, like all other method, still undergoes few restrictions like choice of suitable inlet tool or rather the production of toxic gases inside the plasma chamber. However, the notable characteristics of this method and diversity of possible applications make it a state of interest for researcher team, and gives potential for many future progresses.

CONTENTS

Candidate’s declaration	i
Certificate	ii
Acknowledgement	iii
Abstract	iv
Contents	v
List of figures	vi
List of tables	ix
Chapter 1 Introduction	1
1.1 Motivation	2
1.2 About carbon nanostructures	2
1.3 Applications of carbon nanostructures	4
1.4 Growth techniques	6
Chapter 2 About COMSOL	7
Chapter 3 Literature review	11
Chapter 4 Model	13
Chapter 5 Results and discussions	20
5.1 Variation of pressure	20
5.2 Variation of temperature	31
Chapter 6 Future aspects	42
Chapter 7 Conclusion	43
References	44

List of Figures

Fig 1.1: Schematic presentation of dimensionality of sp2 -hybridized carbon nanostructures. (a) Fullerene (0D); (b) carbon nanotube (CNT) (1D); (c) graphene nano ribbon (1D); (d) graphene sheet (2D); (e) graphite (3D); (f) 3D CNT networks (3D); (g) hybrid of graphene with horizontal CNT (hCNT) (3D); (h) hybrid of graphene with vertical CNT (vCNT) (3D); and (i) graphene triple periodical minimal surfaces (or schwarzites 3D graphene)

Fig 1.2: Model of carbon nanotube

Fig 1.3: Applications of nanostructures in food science

Fig 1.4: Schematic representation of possible mechanisms of toxicity involved in metal-containing nano-materials: (1) metal ion uptake into cells, (2) generation of reactive oxygen species, and (3) bacterial cell membrane damage. NP = nanoparticle; ROS = reactive oxygen species.

Fig 1.5: Diagram showing the development of nanotechnology in food science/industry and its functionality, applicability, and safety assessments.

Fig 2.1: Comsol interface snapshot 1

Fig 2.2: Comsol interface snapshot 2.

Fig-4.1: Geometry of the plasma chamber

Fig 5.1: Shows electron densities at three different pressures. Respective maximum values being (a) $1.45x10^{13}$ for 10mtorr, (b) $2.23\ x10^{13}$ for 20mtorr and (c) $6.18x10^{13}$ per m^3 for 50mtorr.

Fig 5.2: Shows electron energy densities at three different pressures. Respective values being (a) $5.28x10^{14}$, (b) $1.22\ x10^{15}$ and (c) $4.78\ x10^{15}$ per m^3.

Fig 5.3: Shows electron temperature at three different pressures. Respective maximum values being (a) 25.5 for 10mtorr, (b) 39.1 for 20mtorr and (c) 58.4 eV for 50mtorr.

Fig 5.4: Shows collisional power loss at three different pressures. Respective maximum values being (a) 817 for 10mtorr, (b) 3.4 $x10^3$ for 20mtorr and (c) $2.7x10^4$ W/m^3 for 50mtorr.

Fig 5.5: Shows electric potential at three different pressures. Respective maximum values on the negative side being (a) 76.4 for 10mtorr, (b) 11.6 for 20mtorr and (c) 200 V for 50mtorr.

Fig 5.6: Shows Argon number densities at three different pressures. Respective maximum values being (a) $6.92x10^6$ for 10mtorr, (b) 4.8 $x10^7$ for 20mtorr and (c) $8.34x10^8$ per m^3 for 50mtorr.

Fig 5.7: Shows H+ ion density at three different pressures. Respective maximum values being (a) $1.38x10^{10}$ for 10mtorr, (b) 1.47 $x10^{10}$ for 20mtorr and (c) $9.68x10^{10}$ per m^3 for 50mtorr

Fig 5.8: Shows C_2H_2+ ion densities at three different pressures. Respective maximum values being (a) $2x10^{20}$ for 10mtorr, (b) 1.4 $x10^{21}$ for 20mtorr and (c) $1.7x10^{21}$ per m^3 for 50mtorr

Fig 5.9: Shows C_2H+ ion densities at three different pressures. Respective maximum values being (a) $5.39x10^{10}$ for 10mtorr, (b) 5.75 $x10^{10}$ for 20mtorr and (c) $3.81x10^{11}$ per m^3 for 50mtorr

Fig 5.10: Shows C_2H_3+ ion density at three different pressures. The respective maximum values being (a) $1.36x10^{21}$ for 10mtorr, (b) 2.06 $x10^{20}$ for 20mtorr and (c) $2.5x10^{20}$ per m^3 for 50mtorr.

Fig 5.11: Shows electron densities at two different temperatures. Respective maximum values being (a) $1.45x10^{13}$ for 300K and (b) 7.5 $x10^{12}$ for 723K.

Fig 5.12: Shows electron energy densities at two different temperatures. Respective maximum values being (a) $5.28x10^{14}$ for 300K and (b) $2.15\ x10^{14}$ for 723K.

Fig 5.13: Shows electron temperature (eV) at two different gas temperatures. Respective maximum values being (a) 25.5 for 300K and (b) 20.4 for 723K.

Fig 5.14: Shows collisional power loss at two different temperatures. Respective maximum values being (a) 817 for 300K and (b) 275 for 723K.

Fig 5.15: Shows electric potential (V) on the negative side at two different temperatures. Respective maximum values being (a) 76.4 for 300K and (b) 52.1 for 723K.

Fig 5.16: Shows Argon number densities at two different temperatures. Respective maximum values being (a) $6.92x10^{6}$ for 300K and (b) $1.26\ x10^{7}$ for 723K.

Fig 5.17: Shows H+ ion densities at two different temperatures. Respective maximum values being (a) $1.38x10^{10}$ for 300K and (b) $9.35\ x10^{9}$ for 723K.

Fig 5.18: Shows C_2H_3+ ion densities at two different temperatures. Respective maximum values being (a) $2x10^{20}$ for 300K and (b) $1.94\ x10^{20}$ for 723K.

Fig 5.19: Shows C_2H+ ion densities at two different temperatures. Respective maximum values being (a) $5.39x10^{10}$ for 300K and (b) $3.66\ x10^{10}$ for 723K.

Fig 5.20: Shows C_2H_2+ ion densities at two different temperatures. Respective maximum values being (a) $1.36x10^{21}$ for 300K and (b) $1.32\ x10^{21}$ for 723K.

List of Tables

Table 1.1: Comparison of CVD, PVD and PECVD.

Table 3.1. Summarizes various papers examining the plasma properties

Table 4.1: Materials used for the Simulation Model

Table 4.2: Plasma Parameters

Table 4.3: Different species considered in the Ar/C2H2/H2 model.

Table 4.4: Reactions Involved

1

Introduction

Chemical vapour deposition or CVD in short, is a method for the production of thin films of polymeric materials that has effectively overcome some of the issues confronted by wet chemical fabrication and other deposition methods. There are many hybrid methods that arise from chemical vapor deposition and are continually evolving in order to improve and modify the properties of the fabricated thin films [3]. Amongst them, plasma enhanced chemical vapor deposition or in short, PECVD, is a method that can extend the applicability of the technique for various predecessors, reactive organic and inorganic materials as well as non-reactive or inert materials. Organic or inorganic monomers that are used as predecessors in the Plasma Enhanced CVD, undergo disintegration and radical polymerization while being exposed to a very high-energy plasma stream, followed by thin film deposition. In this chapter, we have given a brief of the history, various characteristics and the major applications of Plasma Enhanced CVD. By indicating the pros and cons of Plasma Enhanced CVD, we have provided an assessment of this technique with other methods.

1.1 Motivation

Nanotechnology is a rapidly emerging field providing users with nanostructures without being tethered off of conventional methods. Carbon nanostructures are being developed to provide high tensile strength, high thermal and electrical conductivity, light weight and flexible and wide range of band gap to users. Nano-materials are being studied as an alternative to the traditional materials as they offer all the above stated advantages, which makes them unique. Physical and environmental necessity is another driving factor in favor of these nano materials.

There exist different methods for production of these nano materials such as sol-gel, laser ablation method, ball milling, sputtering, physical vapor deposition and chemical vapor deposition. Out of them, the most widely used technique is PECVD that is Plasma Enhanced Chemical Vapor Deposition. With many advantages like low temperature, thermal and chemical stability, the major challenges include cost effectiveness, commercial production, etc.

1.2 About Carbon Nanostructures

Allotropes of Carbon

1) Diamond
2) Graphite

Diamond being rigid crystal clear and graphite being soft, lustrous and shiny black.

Carbon60 and other fullerenes were discovered many decades back and carbon nanotubes in 1992 and graphene being the most recently discovered in 2004 have bred great excitement among scientists [10].

The prearrangement of the carbon atoms forming nanostructures make all the difference. Carbon nano-structures may be o dimensional, one dimensional, 2 dimensional or three dimensional. [The figure reference has been taken from White C. T. et al. *Phys. Rev. B* 47, 5485 (1993)]. Quantum dot is the zero dimensional carbon nano-structure, carbon nanotube or CNT is the example of one dimensional carbon nano-structure, graphene is the example of two dimensional carbon nano-structure, and graphite being three dimensional carbon nano-structure.

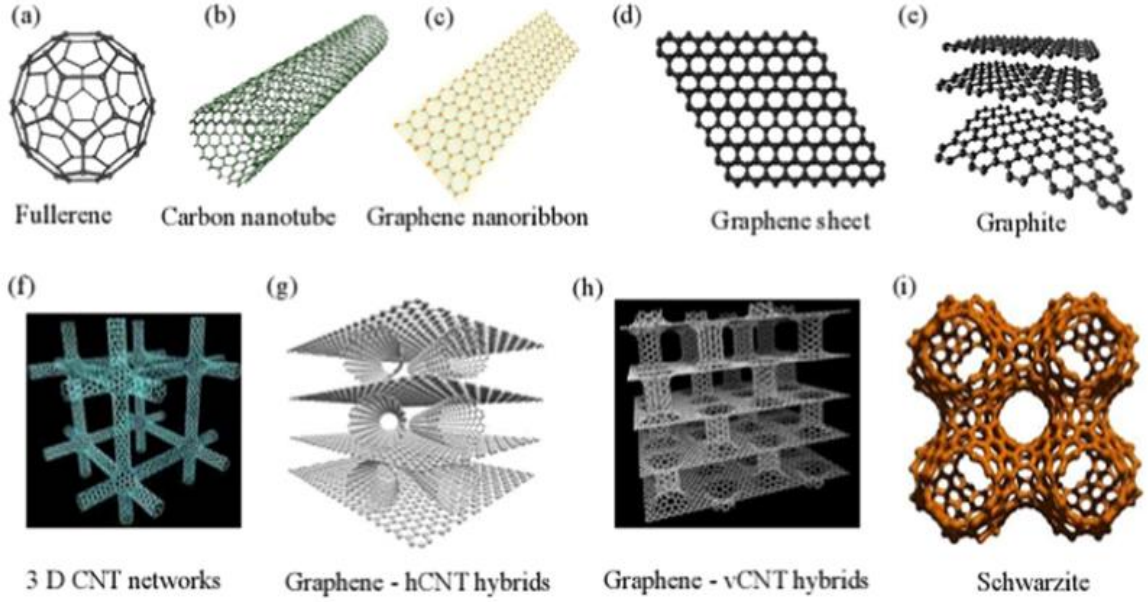

Fig1. Schematic presentation of dimensionality of sp2 -hybridized carbon nanostructures. (a) Fullerene (0D); (b) carbon nanotube (CNT) (1D); (c) graphene nano-ribbon (1D); (d) graphene sheet (2D); (e) graphite (3D); (f) 3D CNT networks (3D); (g) hybrid of graphene with horizontal CNT (hCNT) (3D); (h) hybrid of graphene with vertical CNT (vCNT) (3D); and (i) graphene triple periodical minimal surfaces (or schwarzites 3D graphene) [14].

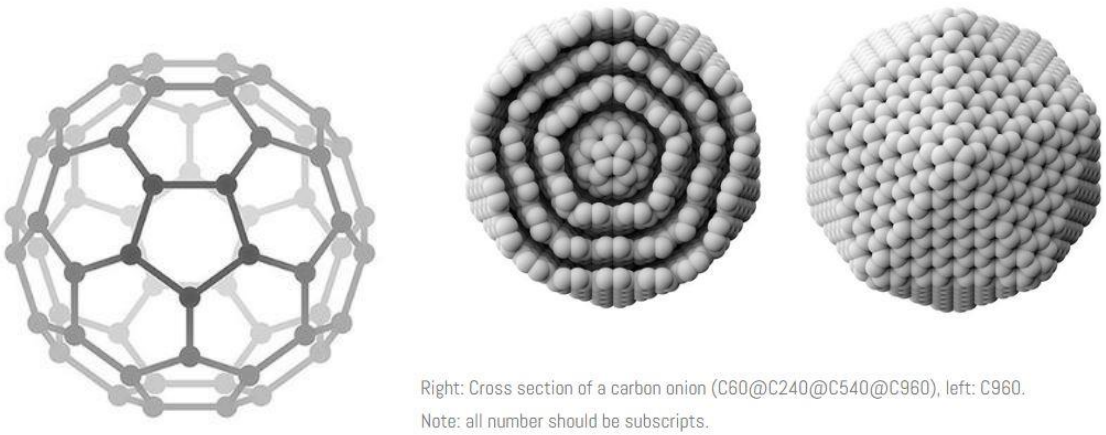

Right: Cross section of a carbon onion (C60@C240@C540@C960), left: C960.
Note: all number should be subscripts.

Carbon nanotubes are basically cylindrical shaped nanostructures that is an allotrope of carbon. These structures possess unique and uncommon properties that are extremely important for nano scale engineering. It offers extra-ordinary strength and that is nearly magical in nature [8]. It is due to the fact that the diameter to length ratio for carbon nano-

tube is approx. 1:130000000. Moreover, it offers exceptional properties like extraordinary thermal conductivity.

Basically, the fullerene family constitute the carbon nanotube. It forms single or multi-walled zigzag nanotube of carbon.

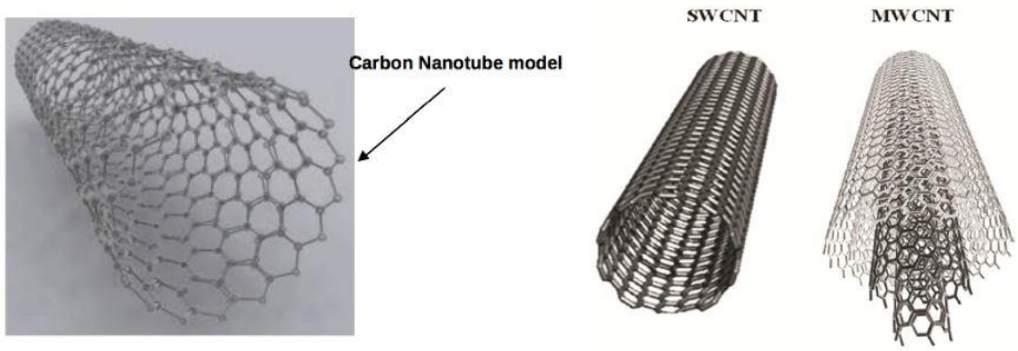

Fig 1.2: Model of carbon nanotube [14].

1.3 Applications

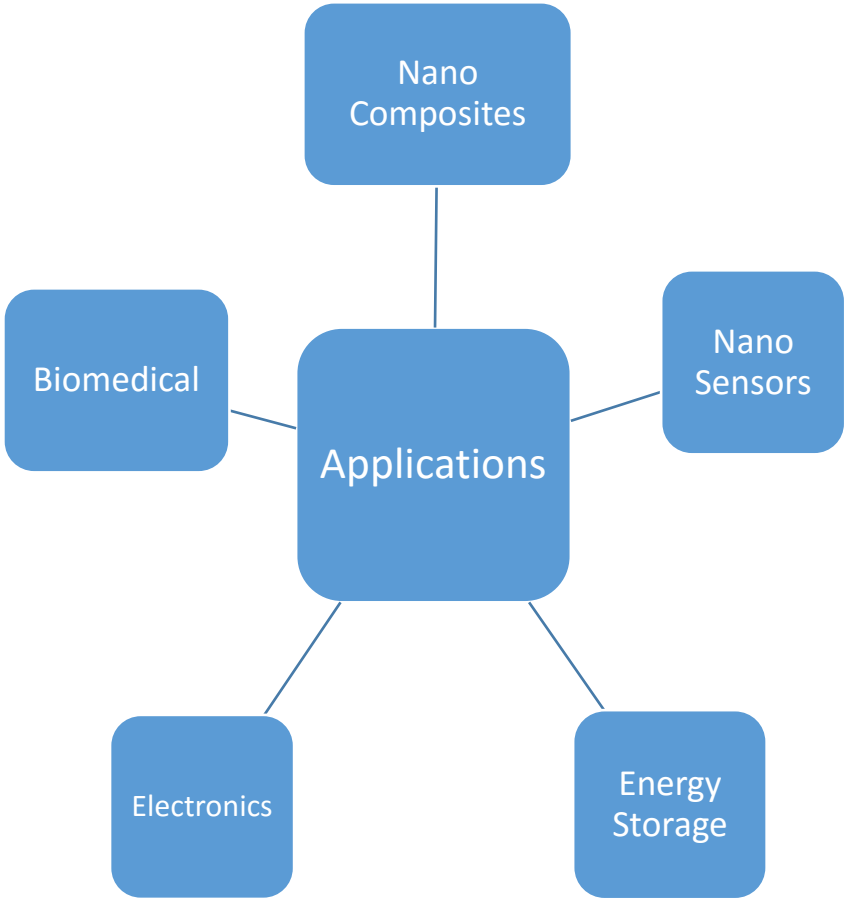

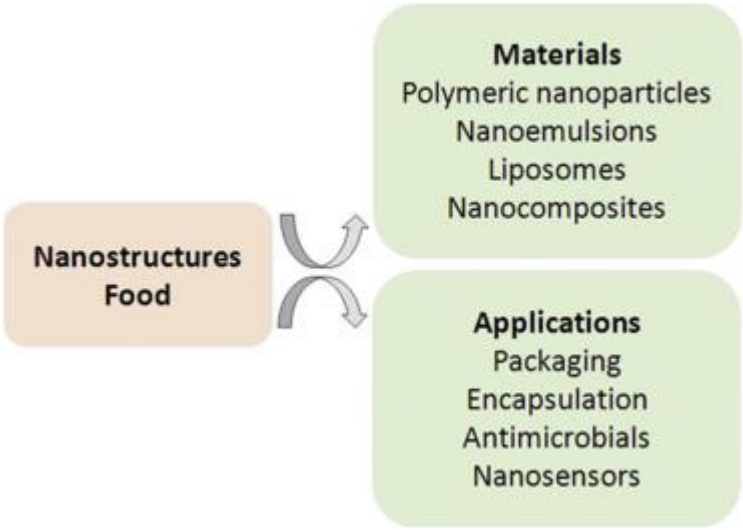

Fig 1.3: Applications of nanostructures in food science [33].

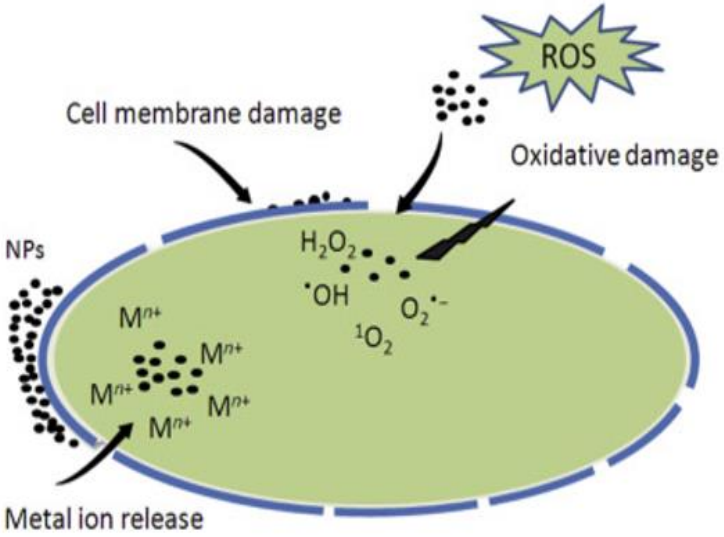

Fig 1.4: Schematic representation of possible mechanisms of toxicity involved in metal-containing nano-materials: (1) metal ion uptake into cells, (2) generation of reactive oxygen species, and (3) bacterial cell membrane damage. NP = nanoparticle; ROS = reactive oxygen species [33].

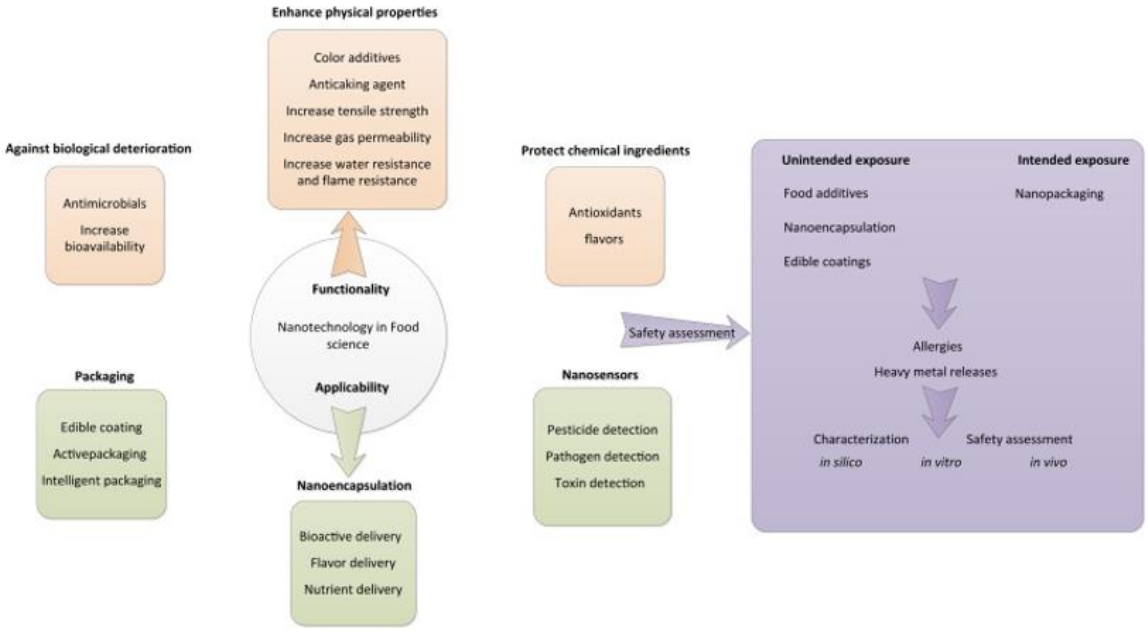

Fig 1.5: Diagram showing the development of nanotechnology in food science/industry and its functionality, applicability, and safety assessments [33].

1.4 Growth techniques

CVD	PVD	PECVD
ADVANTAGES • High deposition rate • Production of thick coating layers • Co-deposition of material at the same time **DISADVANTAGES** • Requirement of high temperatures • Possibility of toxicity of precursors • Mostly inorganic materials have been used	**ADVANTAGES** • Atomic level control of chemical composition • Not requiring the usage of special precursors • Safer than CVD due to the absence of toxic precursors or by-products **DISADVANTAGES** • Line-of-sight deposition • Low deposition rate • Production of thin coating layers • Requirement of annealing time	**ADVANTAGES** • High deposition rate • Low temperatures • Both organic and inorganic materials as precursors • Unique chemical properties of the deposited films • Thermal and chemical stability • High solvent and corrosion resistance • No limitation on substrates: complicated geometries and composition **DISADVANTAGES** • Instability against humidity and aging • Existence of compressive and residual stresses in the films • Time consuming specially for super-lattice structures • Existence of toxic, explosive gases in the plasma stream • High cost of equipment

Table 1.1: Chemical Vapor Deposition, Physical Vapor Deposition and Plasma Enhanced Chemical Vapor Deposition comparison [1].

2

About COMSOL

This chapter gives the outline of the simulation software used by us, its interfaces and its various components.

The workflow for building a model in COMSOL is as follows:

1. Set up the model environment
2. Create geometrical objects
3. Specify material properties
4. Create the mesh
5. Run the simulation
6. Post process the results

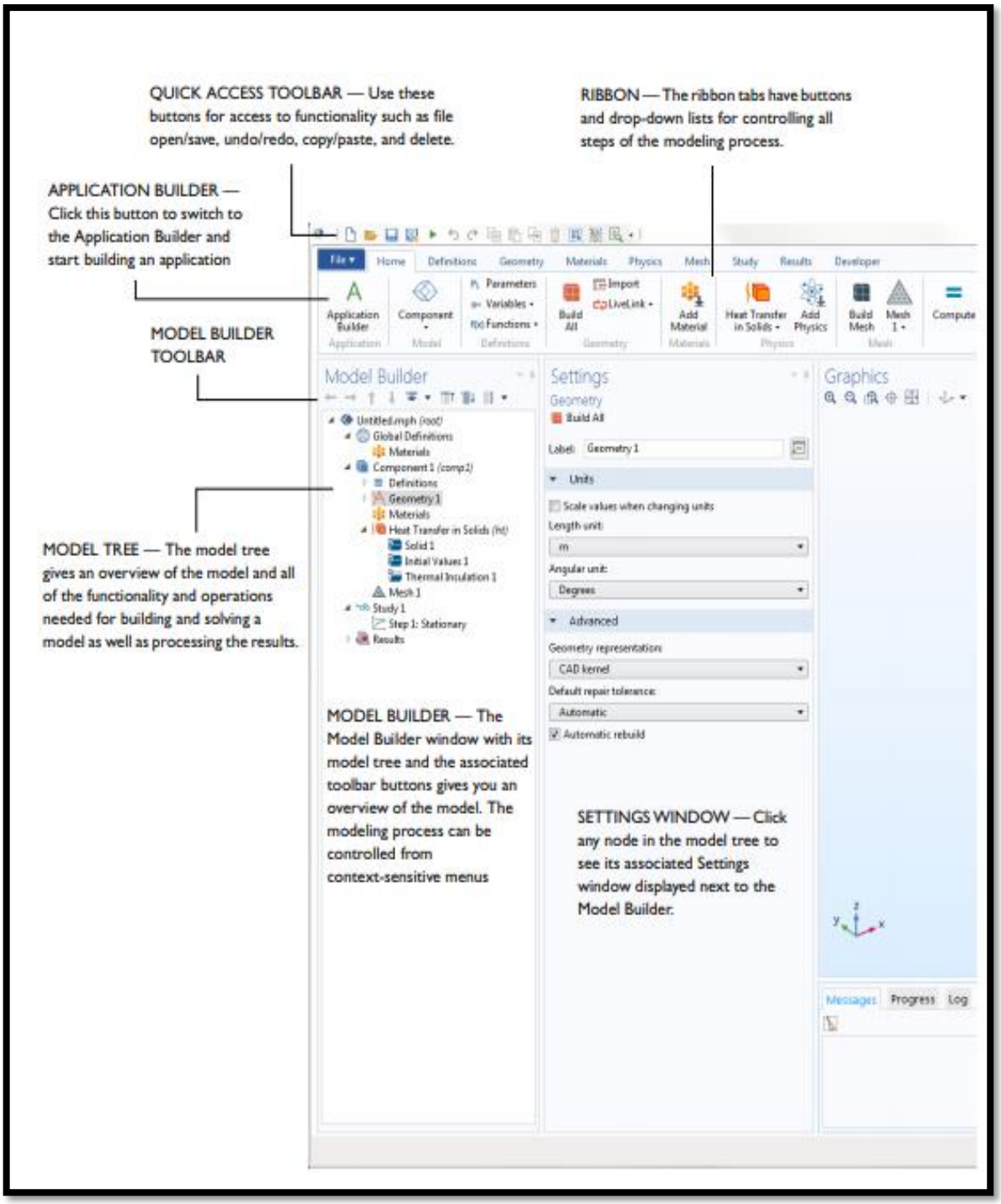

Fig 2.1: COMSOL interface snapshot 1. Image source: COMSOL Multiphysics introduction pdf.

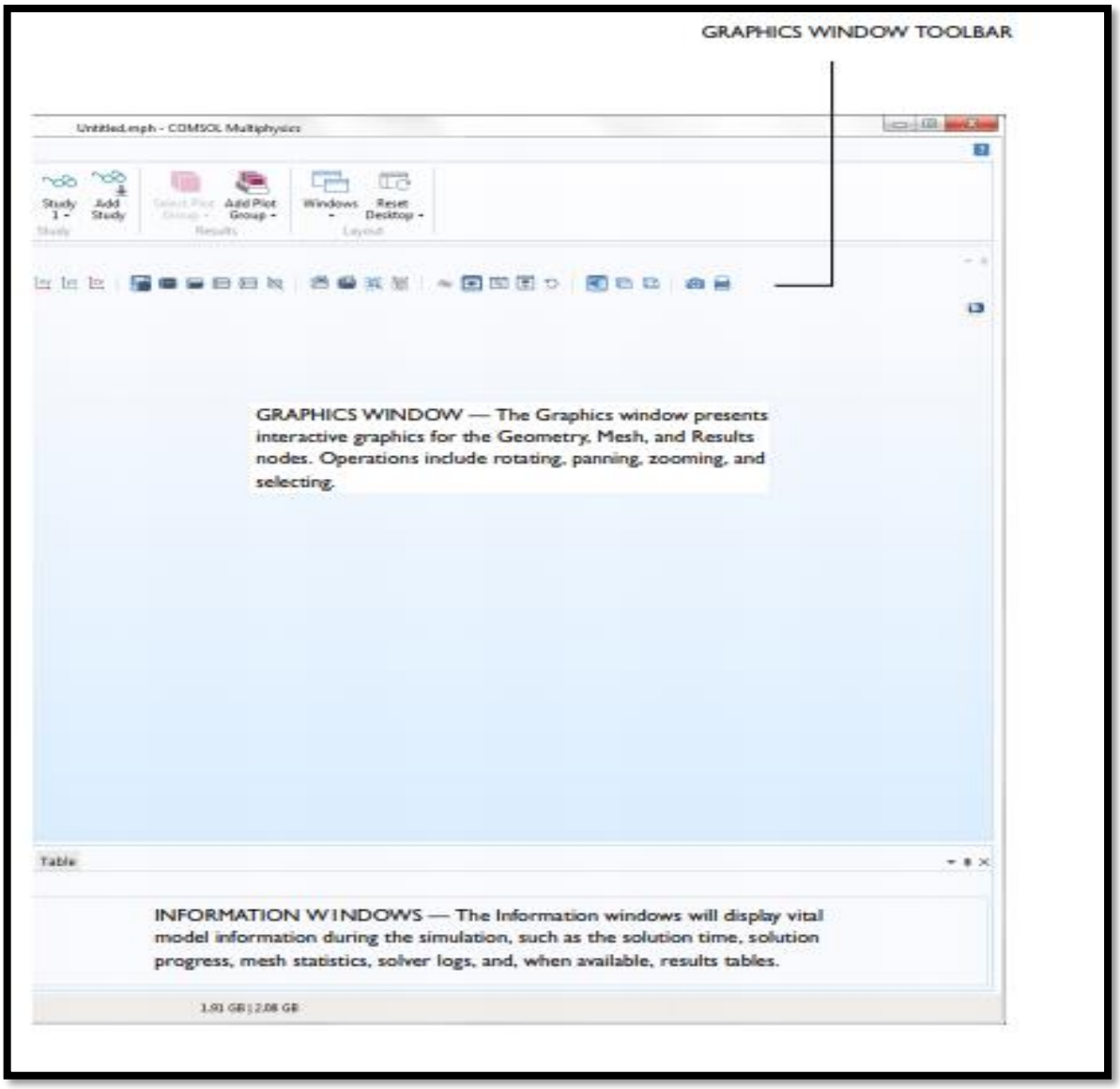

Fig 2.2: COMSOL interface snapshot 2. Image source: COMSOL Multiphysics introduction pdf.

Set up the model environment

There is various type of model environments we can take for the COMSOL simulation in which our model will be studied. The different types of model environment vary from 1-D to 3-D and symmetric model to axis-symmetrical model.

The selection of model environment depends upon the type of study and the results which we want after simulation. For our model we are using 2-D axis-symmetric model for which the geometric structure is symmetric about vertical axis.

Create geometrical objects

COMSOL gives us the flexibility of either drawing the whole 1-D or 2-D or 3-D geometry in the software itself by help of various tools present in the software or directly importing the pre-existing models present at various platform.

One more feature of COMSOL is that one can export or save the geometrical object made using COMSOL geometric tools manually, which can be imported next time for future use and recreational purpose.

Specify material properties

The material section of model builder in COMSOL Multiphysics helps in assigning materials parameters to various domains and boundaries. COMSOL provides a wide range of materials for various physics based modules with options to assign material parameters manually.

Create the mesh

Meshing is one of the most important part in COMSOL for any physics. Boundary surface meeting on the reactor walls is nearly always necessary. It causes the electrons and ions to be captured close to wall in order to resolve the skin depth, fine mesh are always taken.

Run the simulation

After performing all the steps and defining all the physics, materials and mathematics to the system the computation process is started.

Before starting the computation, the type of mathematics involving Numerical methods are selected and the initial values and time steps are added in the study section of COMSOL

Post process the results

After successful computation the COMSOL software itself displays various pre-defined results involving the type of physics we added.

In order to add further more results we can manually add various results including 1-D plot and 2-D plot of various variable parameters as per desired.

3

Literature Review

An extensive research is reported in literature giving the brief review for the research technique used in the analysis of plasma parameters. Various techniques like simulation, algorithm, etc.

Table 3.1. Summarizes various papers examining the plasma properties

S NO.	Research Papers	Results	Reference
1.	Investigating the plasma chemistry for the synthesis of carbon nanotubes or nano-fibers in an inductively coupled plasma enhanced CVD system: the effect of different gas mixtures	The plasma properties are discussed for different gas mixtures at low and moderate pressures, and the growth precursors for CNTs/CNFs are analyzed.	M Mao and A Bogaerts

2.	GEC ICP Reactor	The peak electron density occurs at the center of the reactor, underneath the RF coil. The electron density in this case is high enough to cause some shielding of the azimuthal electric field.	Comsol 5.2a Argon chemistry module
3.	Two-Dimensional Simulation of Nano assembly Precursor Species in Ar/H2/C2H2 reactive plasmas.	The results of two-dimensional fluid simulation of number densities and fluxes of the main building blocks and surface preparation species involved in nano assembly of carbon-based nano patterns in ArþH2þC2H2 reactive plasmas are reported	Kostya (Ken) Ostrikov,* Hyun-Jin Yoona, Amanda E. Rider, Sergey V. Vladimirov
4.	Two-dimensional fluid Simulation of an RF Capacitively Coupled Ar/H2 Discharge	Various reactions that occur within RF plasma chamber were considered.	Lizhu Tong
5.	Effect of Gas Flow Rate and Gas Composition in Ar/CH4 Inductively Coupled Plasmas	The properties in low pressure inductively coupled Ar/CH_4 plasmas operating at an RF frequency of 13.56 MHz and total gas pressure of 20 mTorr are studied in this work	L. Tong

4

Model

In the present simulation model, the growth of graphene is studied in $Ar/C_2H_2/H_2$ reactive plasma using COMSOL Multiphysics 5.2a modeling suite. The methodology adopted in the simulation involves three physical stages.

1) Plasma Interface, involves the ionization of gas mixture due to the transformer action caused by the inductively coupled plasma action by RF coils. This ionization leads to electron generation followed by series of electron impact reaction.

2) Heavy Species Transport, involves the exposure of carbon-containing gases with plasma in order to produce various ions and radicals. It also involves the interaction of plasma species with the catalyst-substrate surface with the catalyst, if any.

3) Magnetic Field, plays an important role in the generation of high power radio frequency wave through coils to initiate ionization of gases to form the plasma by inductive effect.

These physical interfaces are coupled in the 2D axis symmetric geometry constructed in the Inductively Coupled Plasma (ICP) module in COMSOL Multiphysics 5.2a, as shown in Fig.1. We have developed a two-dimensional PECVD model of plasma of complex $Ar/C_2H_2/H_2$ gas mixtures at low-pressure 20mTorr and low temperature below 723K.

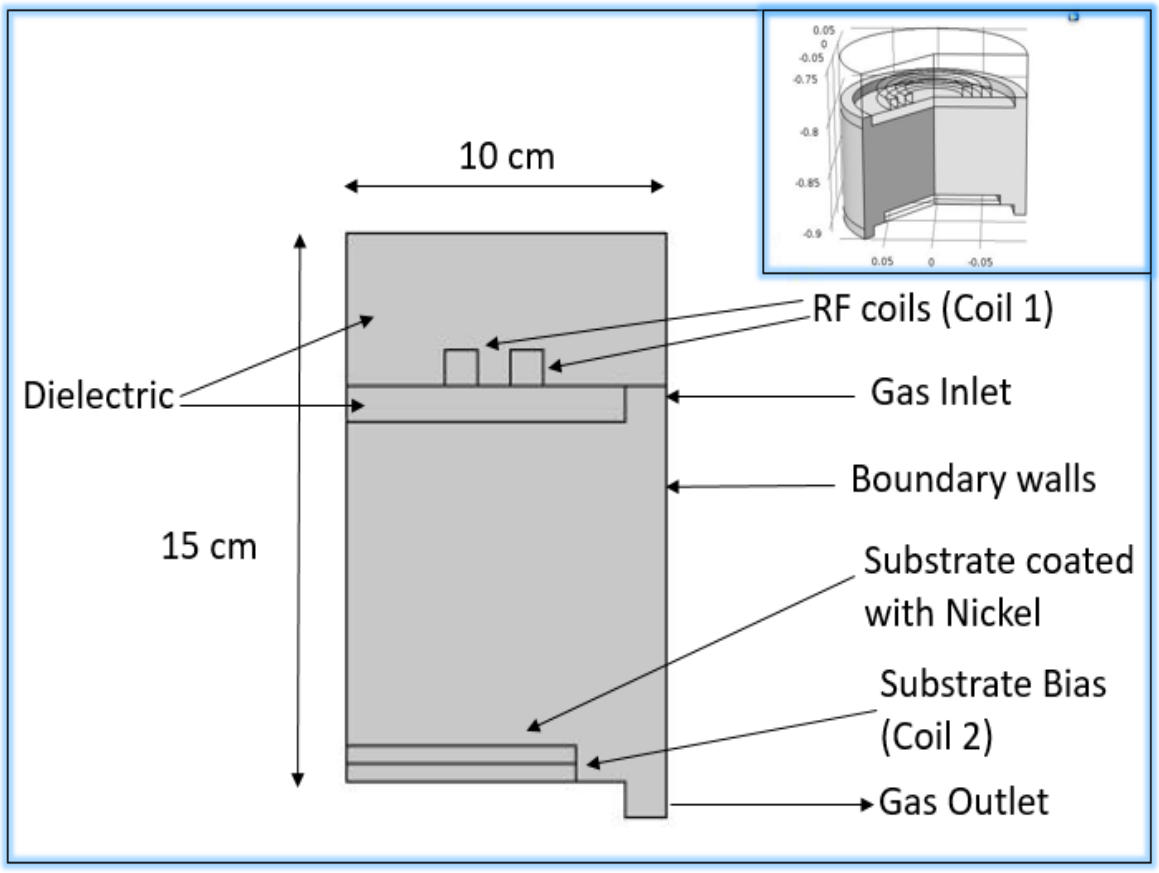

Fig-4.1: Geometry of the plasma chamber

The basic assumptions in the model formulation are: (i) for analysis purpose the actual 3D model is taken as a 2D axis-symmetric geometry, (ii) The dielectrics are taken as insulators to electrically decouple plasma chamber and the coils, (iii) Operating conditions in the chamber are assumed uniform, (iv) Frequency transient study of the system is analyzed using COMSOL Multiphysics 5.2a, (v) Convection of heavy species present in a plasma can often be neglected due to the low operating pressure, (vi) The surface loss (boundary walls) of hydrogen atoms is assumed to be zero, (vii) The electron emission due to ion impact is set to zero and ions are considered as completely absorbed/ neutralized when they arrive at the chamber boundary with the only transitional change in the state of Ar, (viii) The excited hydrogen atoms and argons are set to revert to their ground states when they contact with the walls.

A half 2D axis-symmetric geometry [20] of the side view of the actual Plasma Enhanced Chemical Vapor Deposition chamber was designed in COMSOL Multiphysics v5.2 (COMSOL AB, Stockholm, Sweden) as shown in FIG. 1, which is used to simulate the

various sets of operating conditions. The schematic 3D PECVD model is shown in the inset of FIG. 1, which represents the actual model.

In FIG. 1, the plasma reactor chamber consists of a metal cylinder of radius 10 cm and height 15 cm. A substrate platform of radius 7 cm is placed 8 cm below the chamber top. A four-turn spiral antenna [20] (inductive coil) named Coil 1 is located at the top of the chamber and is connected to a 13.56 MHz generator. This RF coil is the main source for ICP plasma source. The antenna configuration with only four coil turns was chosen intentionally to generate low-temperature plasmas with non-uniform density profiles along the radial direction [20]. A negative substrate bias named coil 2 is also provided beneath the substrate consisting of DC voltage source with biasing ranged from -10 V to -400 V DC. Insulators around high power magnetic coils to electrically isolate them from the surrounding and plasma chamber with materials defined in TABLE I, Inlet and outlet are provided to supply gases into the plasma chamber. A silicon (100) coated substrate is taken for the plasma-assisted growth over it.

TABLE 4.1: Materials used for the Simulation Model

Medium	Electrical Conductivity	Relative Permittivity	Relative Permeability
RF coils (Coil 1)	$6x10^7$ S/m	1	1
Dielectrics/Insulators	0	1	4.2

Meshing is a critical step in plasma model which is needed to capture the separation of space- charge between the electrons and ions close to the wall. Inductively coupled plasma and heavy species transport is computationally meshed using COMSOL Multiphysics v5.2a (COMSOL AB, Stockholm, Sweden). The material and spatial domains are meshed using finer boundary layer mesh based on the COMSOL physics-controlled mesh of minimum quality of 0.001m. The plasma chamber domains are meshed using extra fine element size with the free triangular entity. The boundary layer property involved a total of 5 boundary layers with the stretching factor of 1.4.

In this Simulation, the numerical modeling of reactive CVD process is carried out using COMSOL. The model involves the solution of multiple plasma and surface reaction equations for a number of reactants and intermediate species. These reaction equations are provided with tens of finite rate reaction steps and varying rate coefficients. The solution of such rigid sets of equations is difficult and the inbuilt solver of COMSOL does the job accurately and very fast. COMSOL has an easy to use GUI and different inbuilt equation solver of COMSOL provided with various Multiphysics options.

The model incorporates various physics interfaces. When a time-varying electric current is supplied to the RF coils at 13.56 MHz, it produces a time-varying magnetic field in the plasma chamber filled with gases. As per Lenz's law, a time-varying electric current flows inside the chamber gases in opposite direction to oppose the magnetic field. This electric current in the gas chamber ionizes the Argon gas to form the plasma by transformer action. The Plasma interface is used to study the general plasma parameters as electron density, electric potential, and electron temperature. The Heavy Species Transport interface is a mass balance interface for all non-electron species formed in the plasma chamber. This physics interface also makes it possible to add electron impact reactions, chemical reactions, surface reactions, and species, including charged, neutral, and electronically excited species into the model to simulate the actual reactions taking place experimentally.

The electron transport properties are computed from the reduced transport properties using the equation $\mu_e = \frac{\mu_{red}}{N_n}$, where N_n is the number density and μ_{red} is the reduced mobility of electrons. The cross-section data is used to define source coefficients in the model, here the Maxwellian electron energy distribution function (EEDF) is used to define source coefficients $f(\varepsilon) = \varphi^{-\frac{3}{2}}\beta_1 \exp(-(\frac{\varepsilon\beta_2}{\varphi}))$, where $\beta_1 = \Gamma(\frac{5}{2})^{\frac{3}{2}}\Gamma(\frac{3}{2})^{-\frac{5}{2}}$, $\beta_2 = \Gamma(\frac{5}{2})\Gamma(\frac{3}{2})^{-1}$, φ is the mean electron energy in eV, ε is the electron energy in eV, and Γ is the incomplete gamma function.

$$\frac{\partial}{\partial t}(n_e) + \nabla.\Gamma_e = \mathrm{R}_e, \tag{1}$$

$$\frac{\partial}{\partial t}(n_e) + \nabla.\Gamma_e + E.\Gamma_e = \mathrm{R}_\mathrm{e}, \tag{2}$$

$$\Gamma_e = -n_e(\mu_e E) - D_e \nabla n_e, \tag{3}$$

$$\mathrm{R}_\mathrm{e} = \sum_{i=1}^{M} X_i K_i N_n n_e, \tag{4}$$

COMSOL Multiphysics solves a pair of drift-diffusion Eqs. 1 & 2 as equation of Continuity for the electron density and electron energy density respectively, where Γe is the flux of diffusing electron calculated using Eq. 3 termed as Fick's law of diffusion, where D_e is the diffusion constant.

R_e is the source term given by Eq. 4, where K_i is the rate coefficient, N_n is the number density of reactants, E is the electric field in the chamber and n_e is the electron density. The plasma potential is computed from Poisson's equation $-\nabla.\varepsilon_o\varepsilon_r\nabla V = \rho$. The space charge density ρ is computed from the number densities of electrons and other charged species by Eq. 5.

$$\rho = q(\sum_{k=1}^{M} Z_k n_k - n_e), \tag{5}$$

Surface reactions can be specified in terms of rate or sticking coefficients. The surface rate constant is determined using Eq. 6.

$$K_{f,i} = (\frac{\gamma i}{1-\gamma_i/2})\frac{1}{(\Gamma_{tot})^m}\sqrt{\frac{RT}{2\pi M}}, \tag{6}$$

γ_i is the sticking coefficient given by $\gamma_i = a_1 T^{b1}\exp(-\frac{e_i}{RT})$, where M is the mass of species, R is the gas constant, T is the temperature, and a_1 and b_1 are constants.

The carbon species generated over the catalyst substrate surface via various reactions diffuse along the substrate interface. Hence, the velocity of the interface can be mathematically expressed by an equation $v_y = \frac{\vec{j}_m.n_y}{\rho_{carbon}}$, where v_y is the interface velocity and $\vec{j}m.ny$ is the mass flux in the y-direction and ρ_{carbon}(= 2.267 g/cm^3) is density of carbon. Hence, the thickness (d) of the segregated carbon material (planar graphene nanofilms) can be calculated by equation $d = vy * t$, where 't' is time.

Using the above plasma module, simulations are performed for $Ar/C_2H_2/H_2$ for plasma operated at the parameters given in TABLE 2. The plasma species, bulk reactions between various plasma species and surface reactions considered in the present computation are listed in TABLE 3 and TABLE 4 respectively.

The species and chemical reactions considered in the simulation are justified in order to generate 2D analysis of the number densities and fluxes of various species involved, which are vital for Nano assembly of selected carbon-based nanostructures, also to incorporate the essential channels of creation and destruction/sink of such species, and economically and time-based, stay within a reasonable computational cost. For this reason, higher hydrocarbons and other complex radical species were not included in the simulation.

TABLE 4.2: Plasma Parameters

Parameters	**Value**
Input Plasma Power	1500 W
Reduced Electron Mobility	$4x10^{24}$ /V.m.s
Area of the substrate	154 cm^2
Initial Electron Density	10^{13} /m^3
Plasma Power frequency	13.56 MHz (Radiofrequency)
Initial Density of Gases	10^{13} /m^3

TABLE 4.3: Different species considered in the Ar/C2H2/H2 model.

Molecules	Ions	Radicals
Ar	Ar+, ArH+	Ars
C2H2	C_2H+, C_2H+, C_2H_3+	C_2H, C_2H_3
H2	H+, H_2+, H_3+	H

TABLE 4.4: Reactions Involved

Electron Impact reactions				
No	Reaction	Type	Threshold(eV)	Refs.
1	$e^- + Ar \rightarrow e^- + Ar$	Elastic	0	22,23
2	$e^- + Ar \rightarrow e^- + Ars$	Excitation	11.5	22,23
3	$e^- + Ars \rightarrow e^- + Ar$	Super elastic	-11.5	22,23
4	$e^- + Ar \rightarrow 2e^- + Ar^+$	Ionization	15.8	22,23
5	$e^- + Ars \rightarrow 2e^- + Ar^+$	Ionization	4.24	22,23
6	$Ars + Ars \rightarrow e^- + Ar + Ar^+$	Penning Ionization	-	22,23
7	$Ars + Ar \rightarrow Ar + Ar$	Metastable quenching	-	22,23
Plasma chamber Wall Surface reaction				
No	Reaction	Sticking Coefficient		Refs.
8	$Ars \rightarrow Ar$	1		23
9	$Ars^+ \rightarrow Ar$	1		23
Reactions				

No	Reaction	Rate Coefficients (m^3/(s.mol))	Refs.
10	$Ar^+ + C_2H_2 \rightarrow C_2H_2^+ + Ar$	25.29×10^8	24
11	$Ar^+ + H_2 \rightarrow Ar + H_2^+$	0.448×10^8	24
12	$C_2H_2^+ + H_2 \rightarrow C_2H_3^+ + H$	0.1656×10^6	24
13	$H_2^+ + H \rightarrow H^+ + H_2$	1.062×10^7	24
14	$C_2H_2 + H^+ \rightarrow C_2H^+ + H_2$	0.713×10^8	24
15	$C_2H_3^+ + H \rightarrow C_2H_2^+ + H_2$	1.126×10^6	24
16	$C_2H^+ + H_2 \rightarrow C_2H_2^+ + H$	0.182×10^8	24
17	$C_2H_2^+ + H^+ \rightarrow C_2H_2^+ + H_2$	0.713×10^8	24

5

Results and discussions

In the present study, the simulations were performed for two cases (i) at two different temperature: 300 K (representing room temperature) and 723 K. (ii) At three different pressure conditions viz. (a) 10 mtorr; (b) 20 mtorr; (c) 50 mtorr.

Part I: Variation of pressure

Fig. 5.1(a) to 5.1(c) shows the electron densities calculated at constant temperature of 300K and varying the pressures. The peak value of electron density is observed to be $1.45x10^{13}$, $2.23x10^{13}$ and $6.18x10^{13}$ for 10, 20 and 50 mtorr respectively below the power coil (inductive region) in all the cases. Fig. 5.6(a) through Fig. 5.6(c) display the electric potential distribution at these three pressures. Peaks are observed near the coils with the respective values of $5.28x10^{14}$ kg/(ms^{3}A), $1.22x10^{15}$ kg/(ms^{3}A) and $4.78x10^{15}$ kg/(ms^{3}A). The electron energy density is found to be greatest at 50 mtorr.

Fig. 5.5(a) to Fig. 5.5(c) shows the collision power loss distribution in the plasma chamber at three different pressures. When the generated electrons and fluxes of different constituents of gases collide with each other, they tend to transfer their momentum and lose energy in the process [31]. This phenomenon of loss of energy is signified as collision power loss. The maximum collision power loss is 817, 3400 and $2.7x10^4$ at 10, 20 and 50 mtorr respectively.

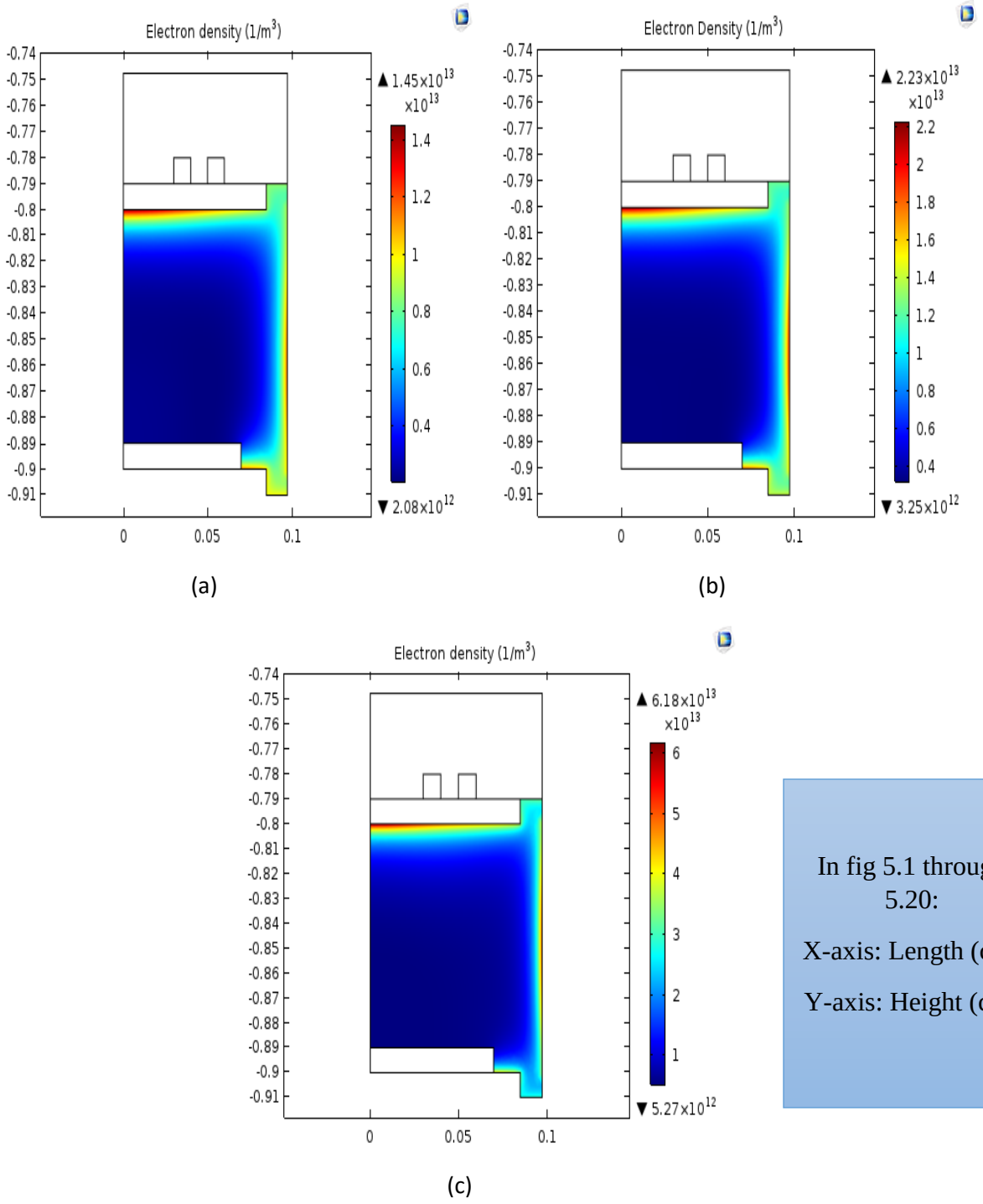

In fig 5.1 through 5.20:

X-axis: Length (cm)

Y-axis: Height (cm)

Fig 5.1: Shows electron densities at three different pressures. Respective maximum values being (a) 1.45×10^{13} for 10mtorr, (b) 2.23×10^{13} for 20mtorr and (c) 6.18×10^{13} per m^3 for 50mtorr.

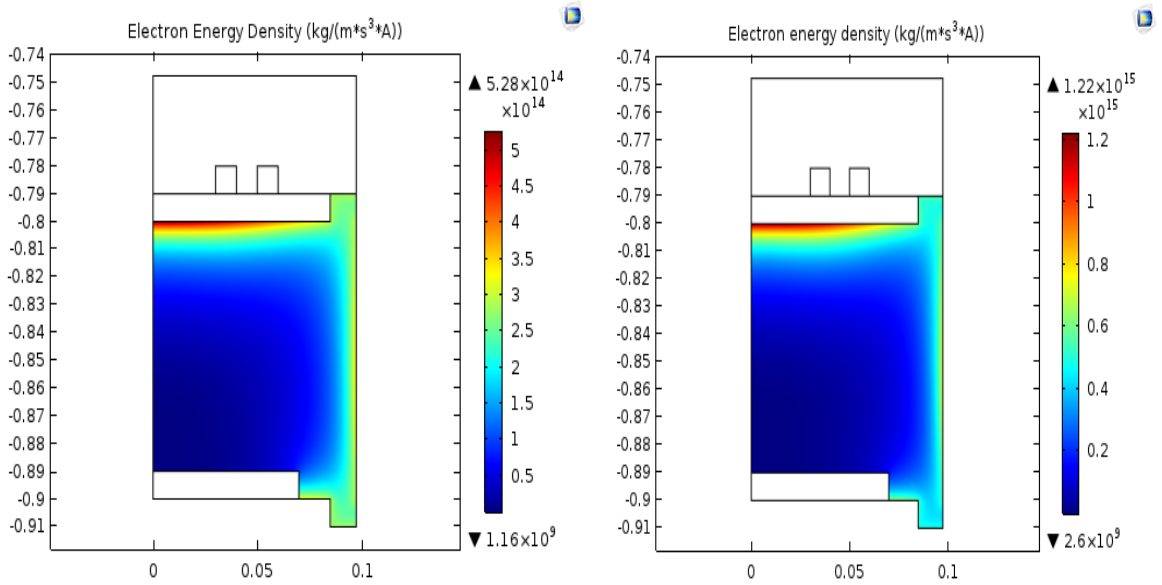

(a)

(b)

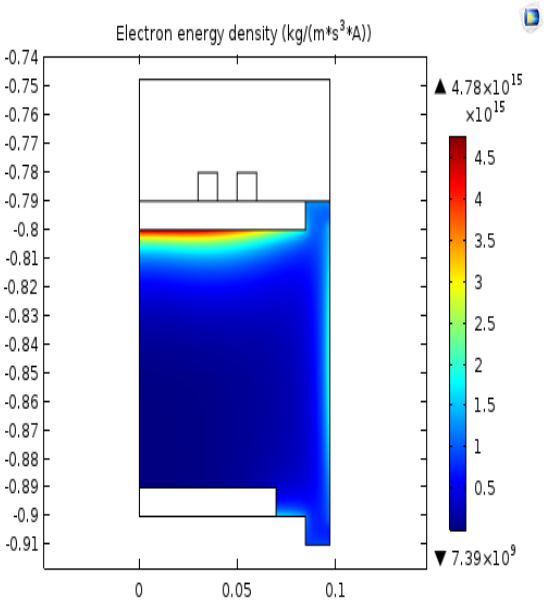

(c)

Fig 5.2: Shows electron energy densities at three different pressures. Respective values being (a) 5.28×10^{14}, (b) 1.22×10^{15} and (c) 4.78×10^{15} per m^3.

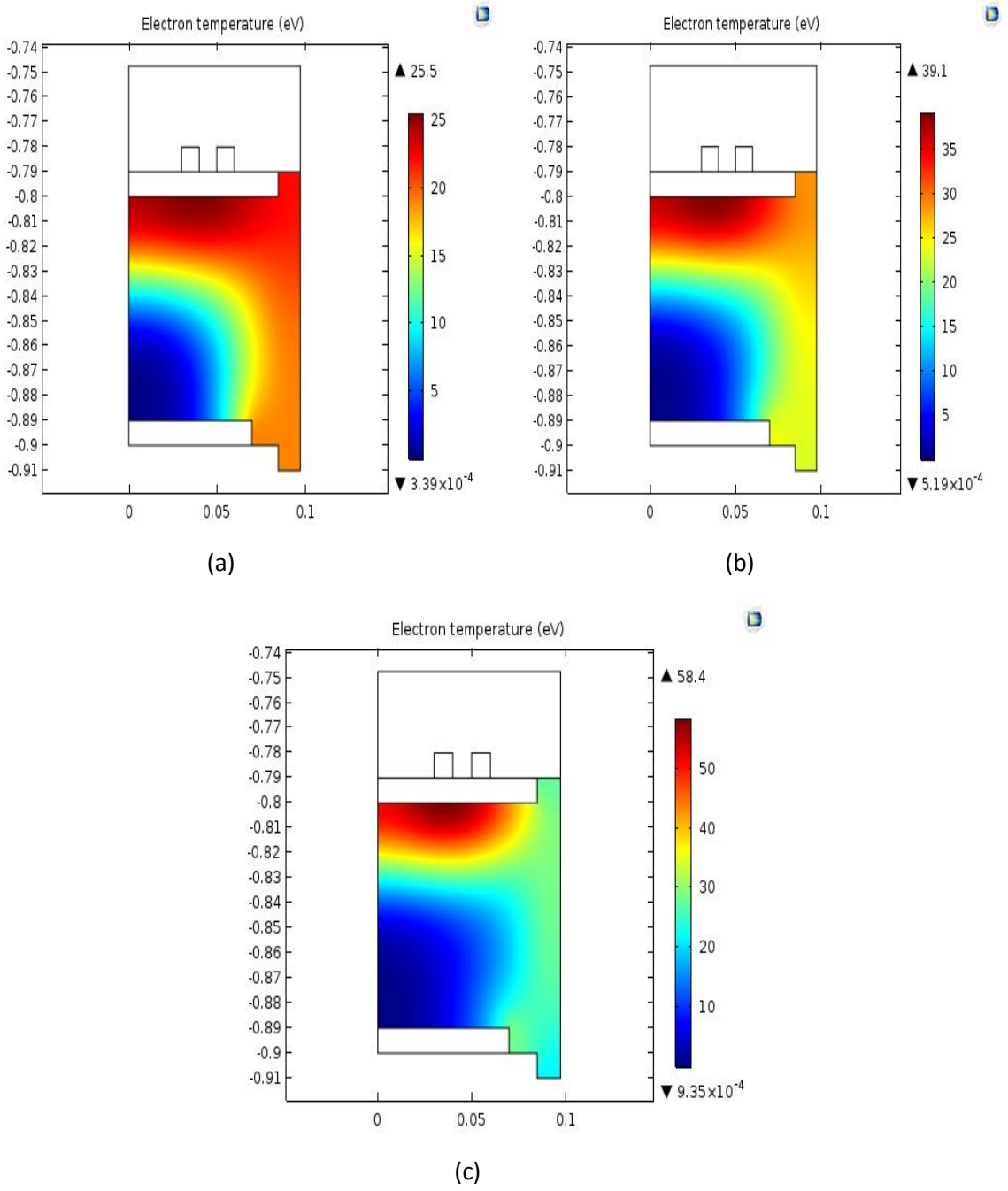

Fig 5.3: Shows electron temperature at three different pressures. Respective maximum values being (a) 25.5 for 10mtorr, (b) 39.1 for 20mtorr and (c) 58.4 eV for 50mtorr.

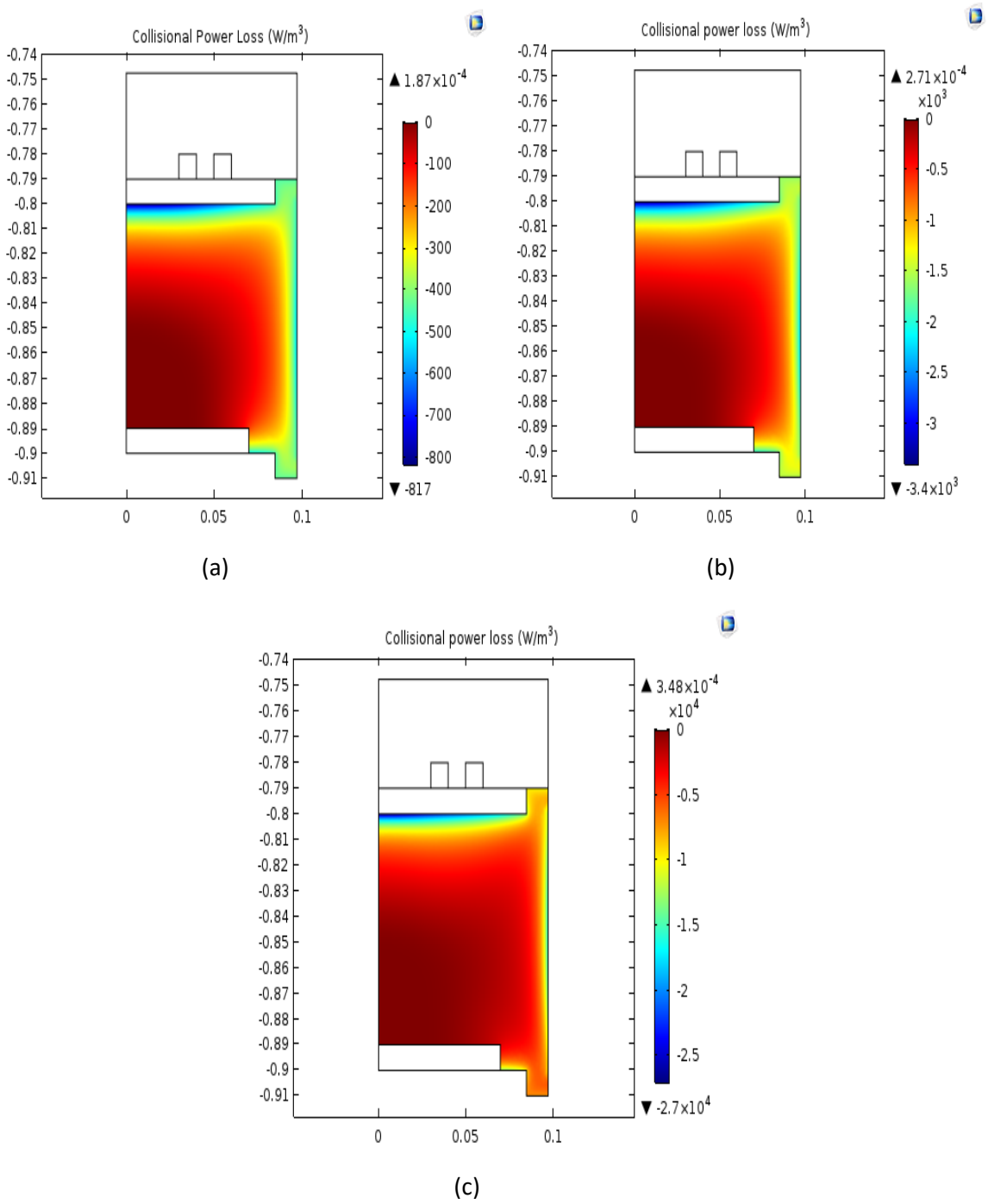

Fig 5.4: Shows collisional power loss at three different pressures. Respective maximum values being (a) 817 for 10mtorr, (b) 3.4 $x10^3$ for 20mtorr and (c) $2.7x10^4$ W/m^3 for 50mtorr.

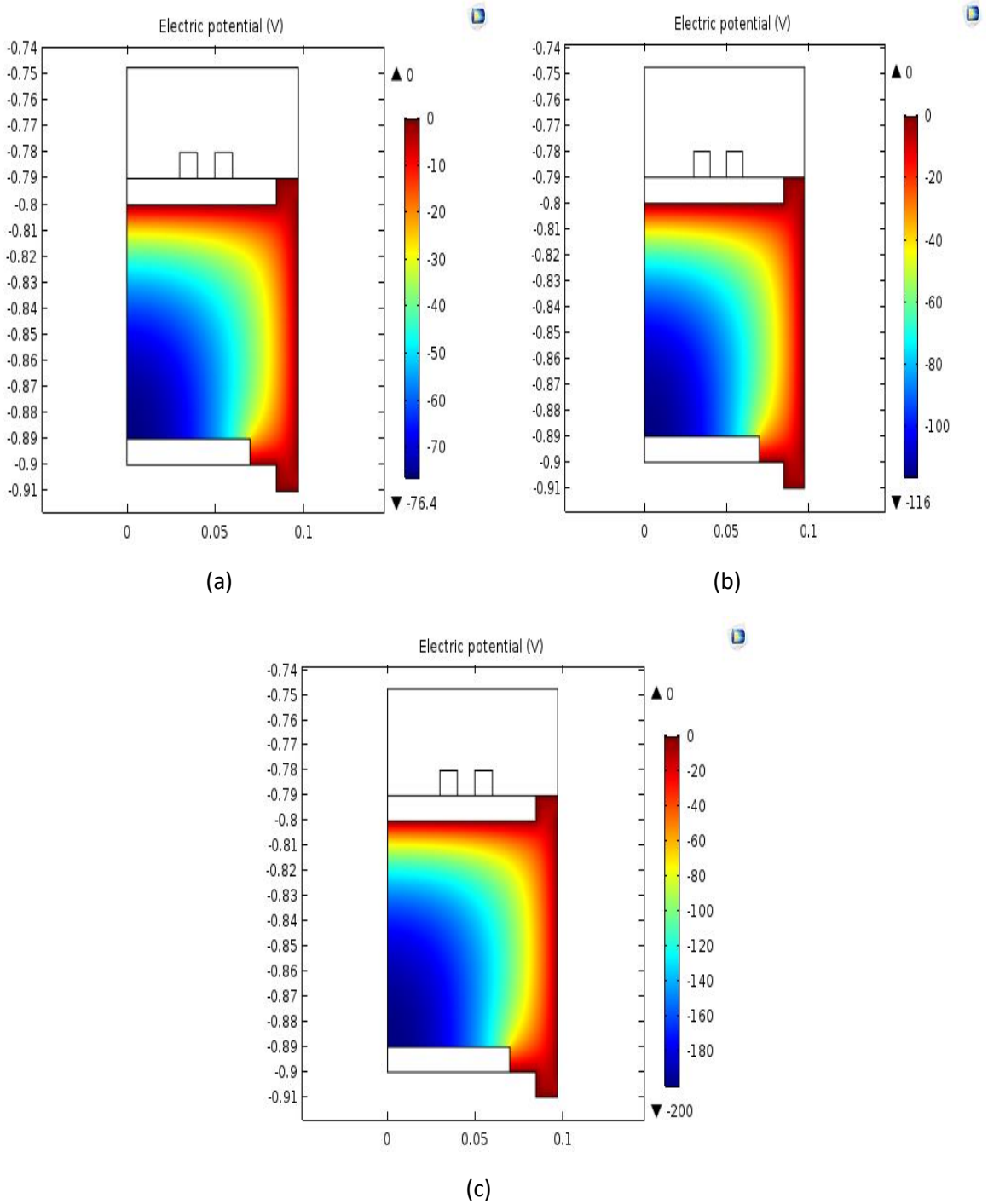

Fig 5.5: Shows electric potential at three different pressures. Respective maximum values on the negative side being (a) 76.4 for 10mtorr, (b) 11.6 for 20mtorr and (c) 200 V for 50mtorr.

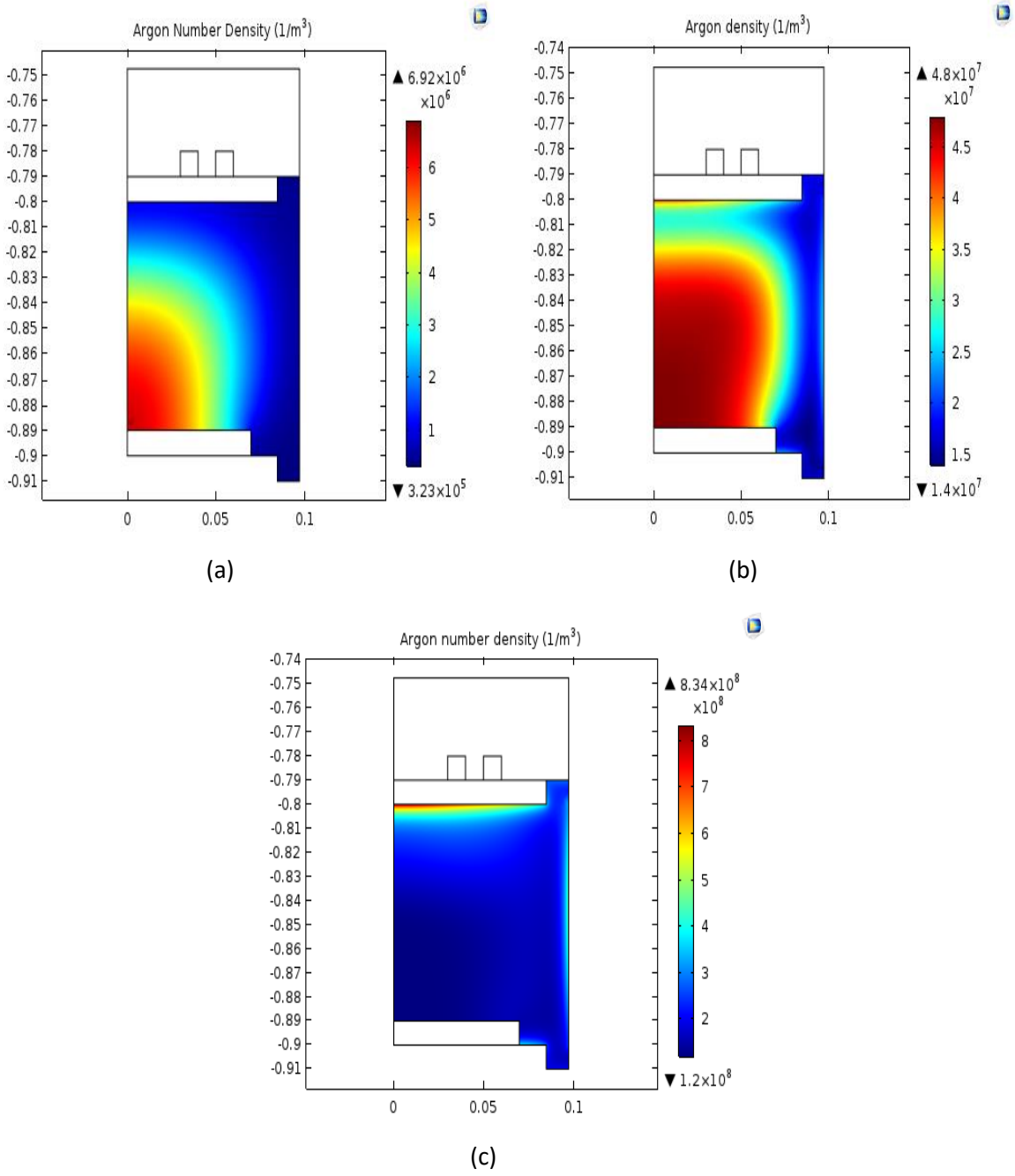

Fig 5.6: Shows Argon number densities at three different pressures. Respective maximum values being (a) 6.92×10^6 for 10mtorr, (b) 4.8×10^7 for 20mtorr and (c) 8.34×10^8 per m^3 for 50mtorr.

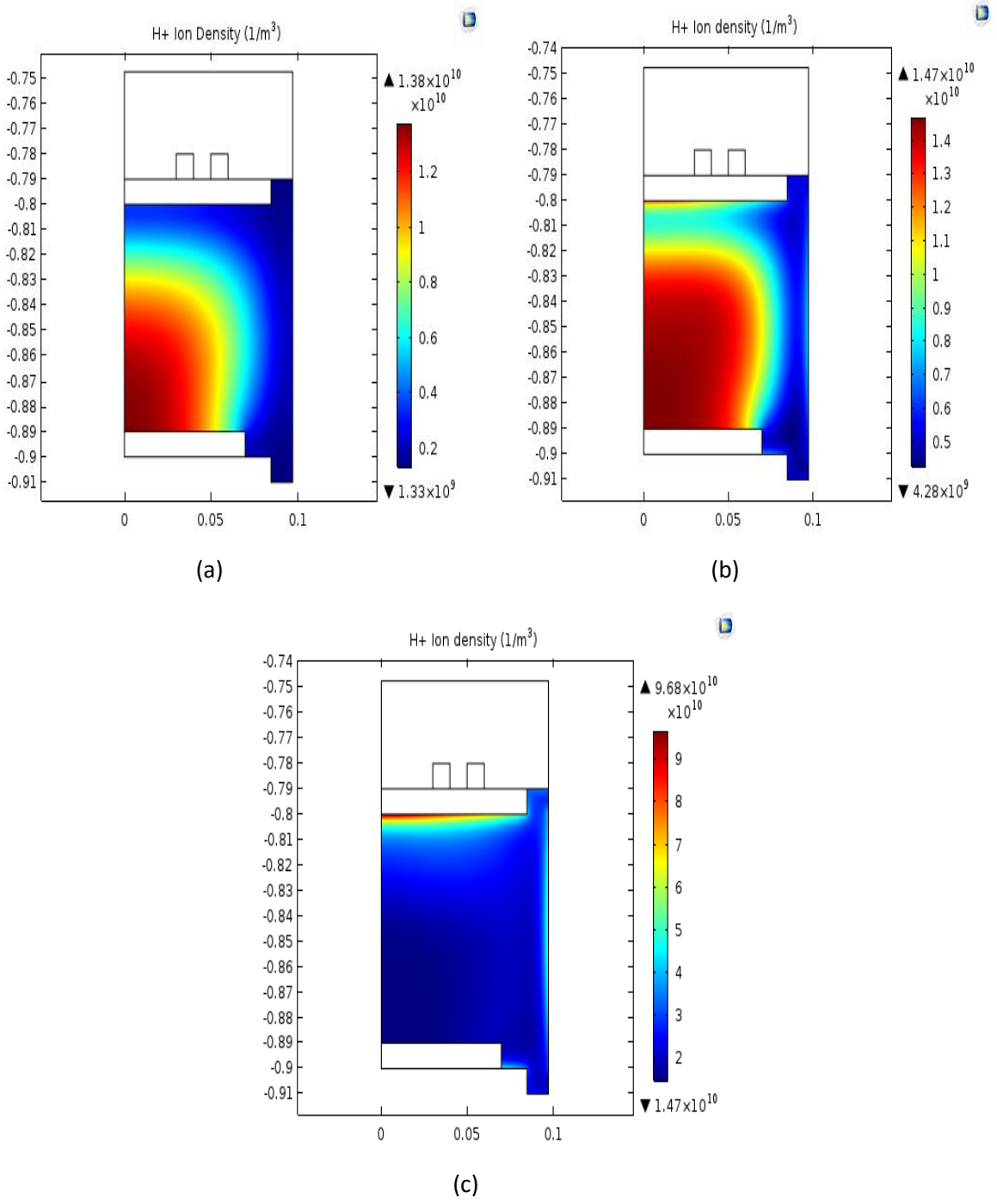

Fig 5.7: Shows H+ ion density at three different pressures. Respective maximum values being (a) 1.38×10^{10} for 10mtorr, (b) 1.47×10^{10} for 20mtorr and (c) 9.68×10^{10} per m^3 for 50mtorr

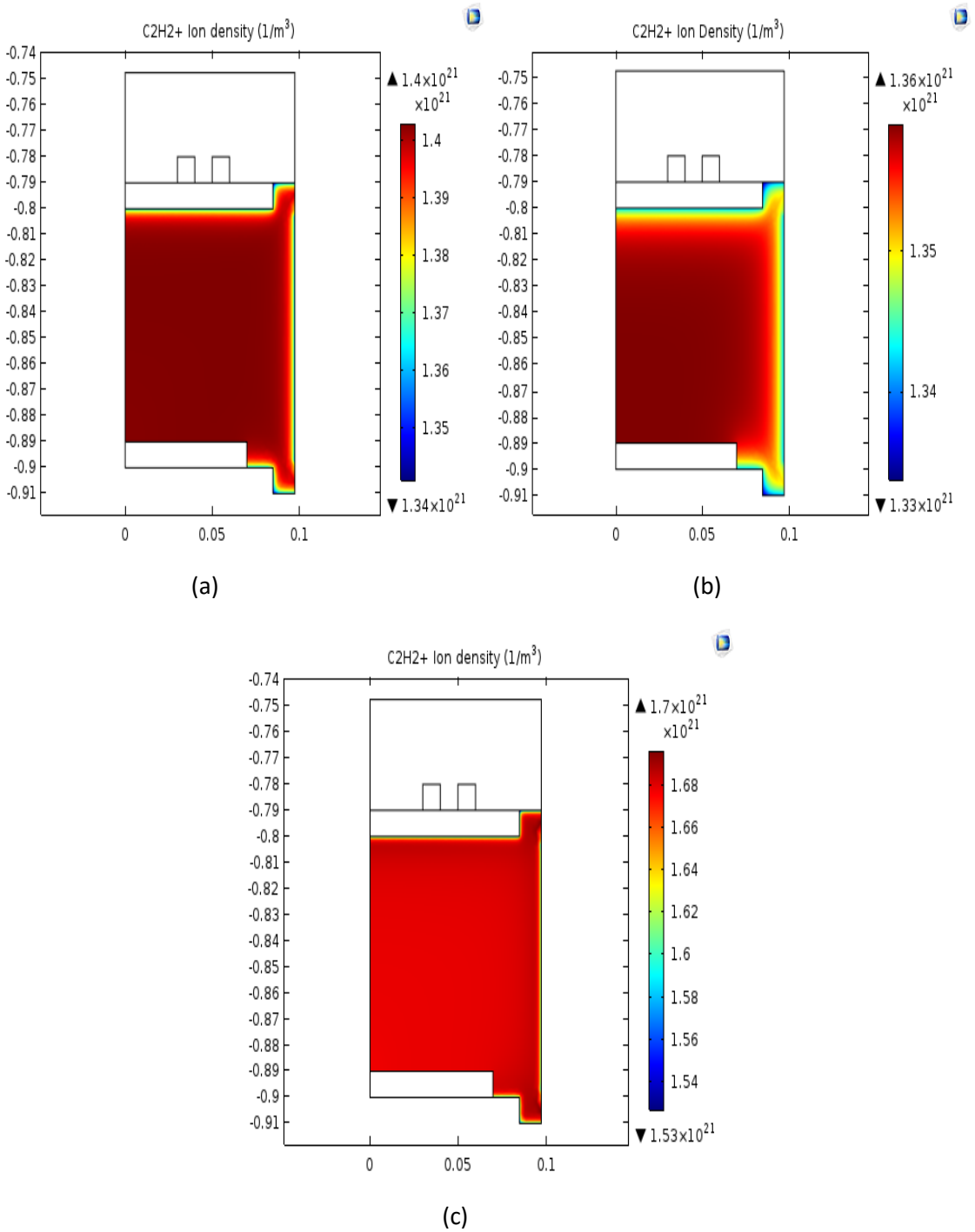

Fig 5.8: Shows C_2H_2+ ion densities at three different pressures. Respective maximum values being (a) $2x10^{20}$ for 10mtorr, (b) $1.4\ x10^{21}$ for 20mtorr and (c) $1.7x10^{21}$ per m^3 for 50mtorr

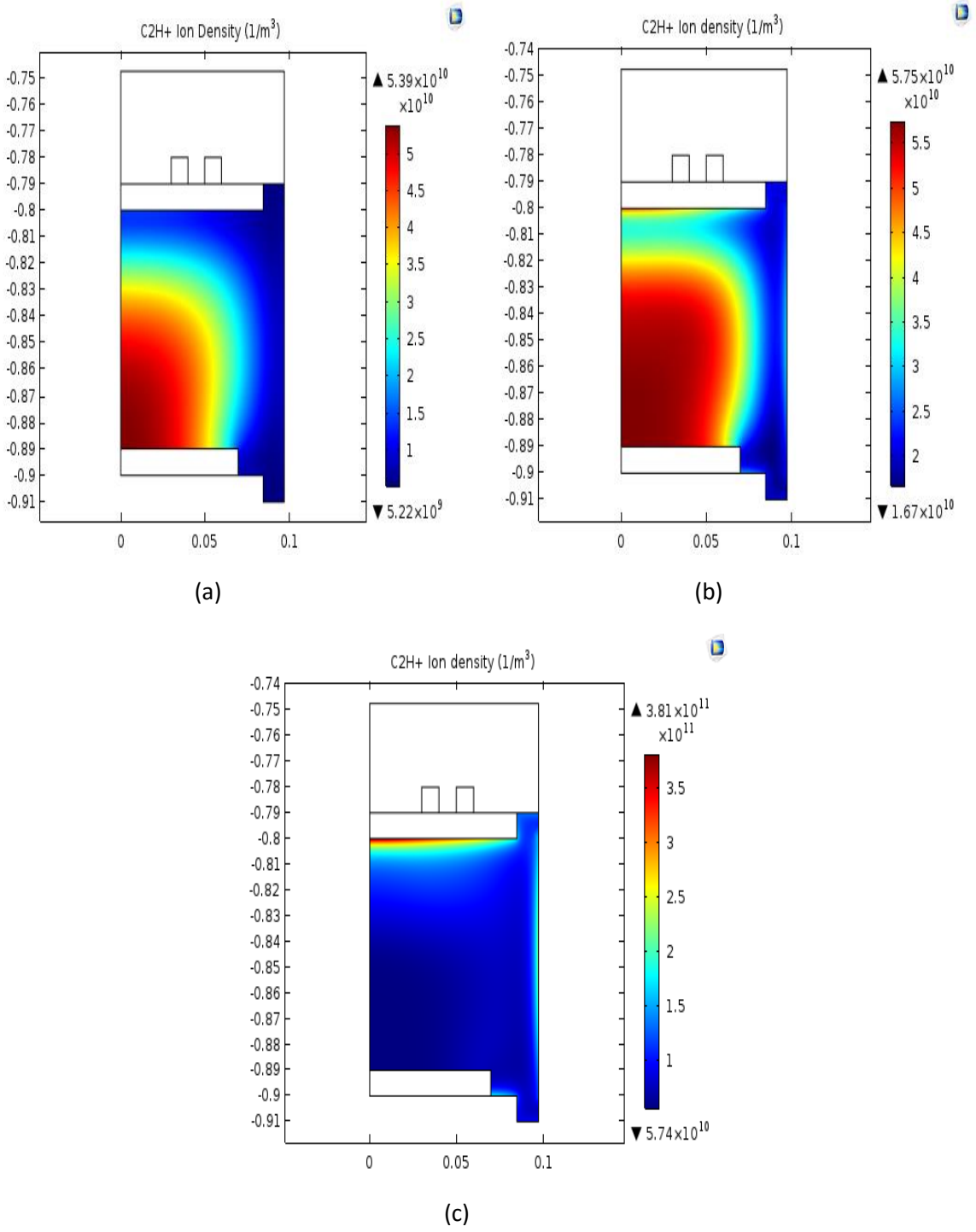

Fig 5.9: Shows C_2H+ ion densities at three different pressures. Respective maximum values being (a) $5.39x10^{10}$ for 10mtorr, (b) $5.75\ x10^{10}$ for 20mtorr and (c) $3.81x10^{11}$ per m^3 for 50mtorr

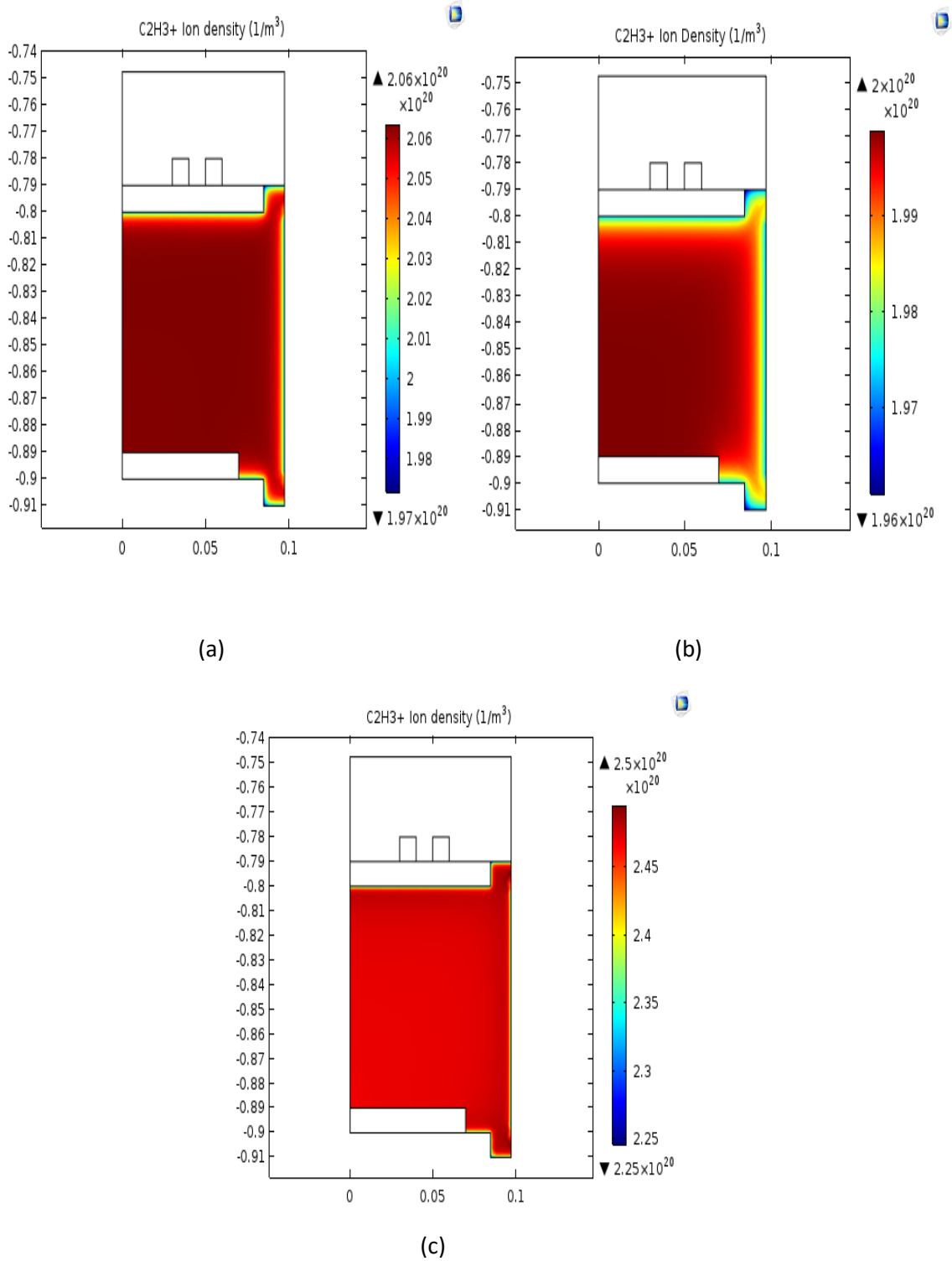

Fig 5.10: Shows C_2H_3+ ion density at three different pressures. The respective maximum values being (a) $1.36x10^{21}$ for 10mtorr, (b) $2.06\ x10^{20}$ for 20mtorr and (c) $2.5x10^{20}$ per m^3 for 50mtorr.

Part 2: Variation of temperature

Figure. 5.11(a) and 5.11(b) shows the electron densities calculated at temperature 300K and 723K respectively at constant pressure of 20 mtorr.

The peak value of electron density is observed to be 2.23×10^{13} and 7.5×10^{12} per m^3 for 300K and 723K respectively below the power coil (inductive region) in all the cases. Fig. 5.16(a) and 5.16(b) display the electric potential distribution at these temperatures. The peak value of electric potential is found to be negative with values 11.6 and 52.1V in the center of the chamber. The distribution of electron energy density are shown in Fig. 5.12(a) and 5.12(b). Peaks are observed near the coils with the respective values of 1.22×10^{15} kg/(ms^3A) and 2.15×10^{14} kg/(ms^3A). The electron energy density is found to be greatest at 300K.

Fig. 5.15(a) and 5.15(b) shows the collision power loss distribution in the plasma chamber at two different temperatures. When the generated electrons and fluxes of different constituents of gases collide with each other, they tend to transfer their momentum and lose energy in the process [31]. This phenomenon of loss of energy is signified as collision power loss. The maximum collision power loss is 3.4×10^3 and 275 at 300K and 723K respectively.

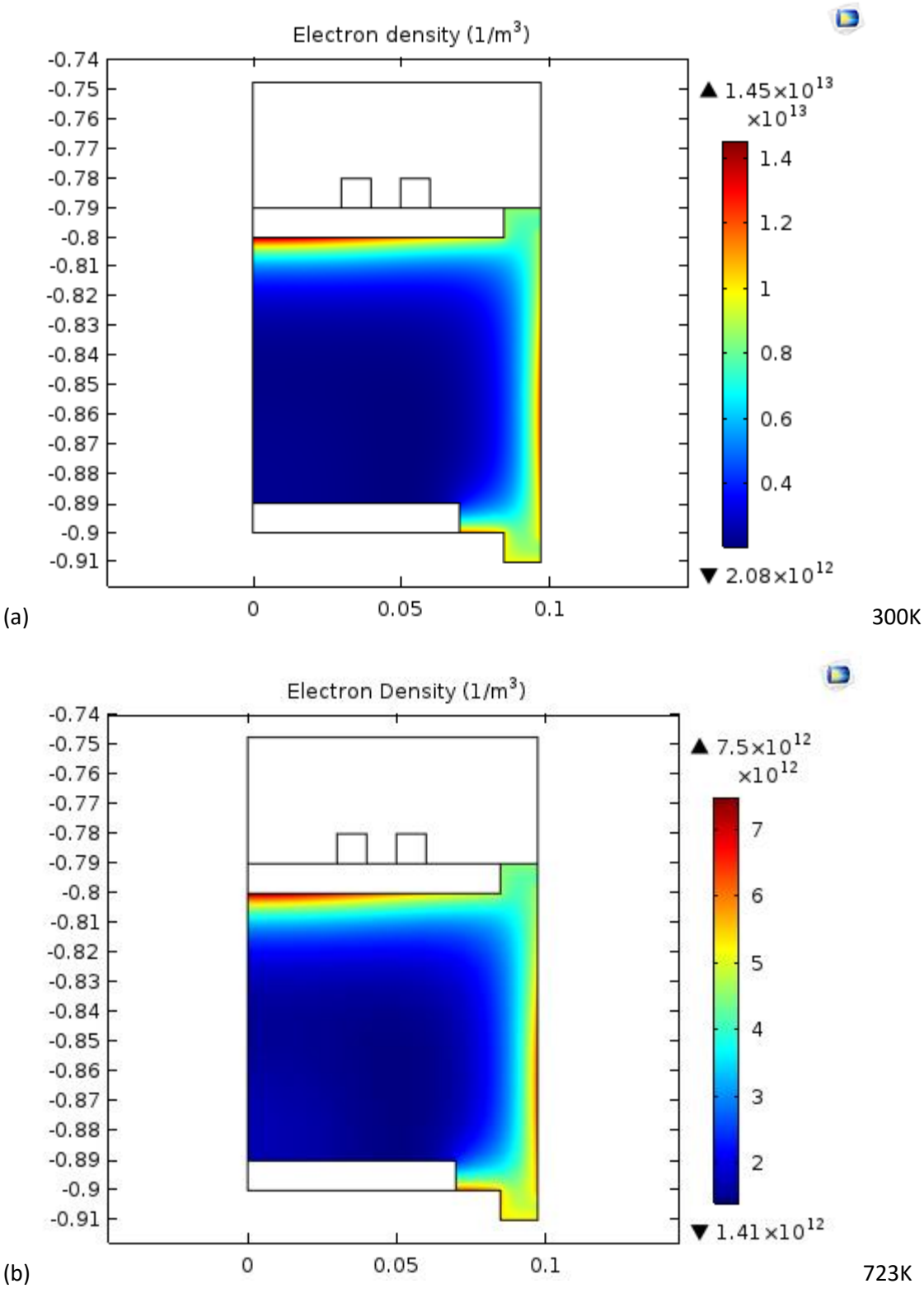

Fig 5.11: Shows electron densities at two different temperatures. Respective maximum values being (a) 1.45×10^{13} for 300K and (b) 7.5×10^{12} for 723K.

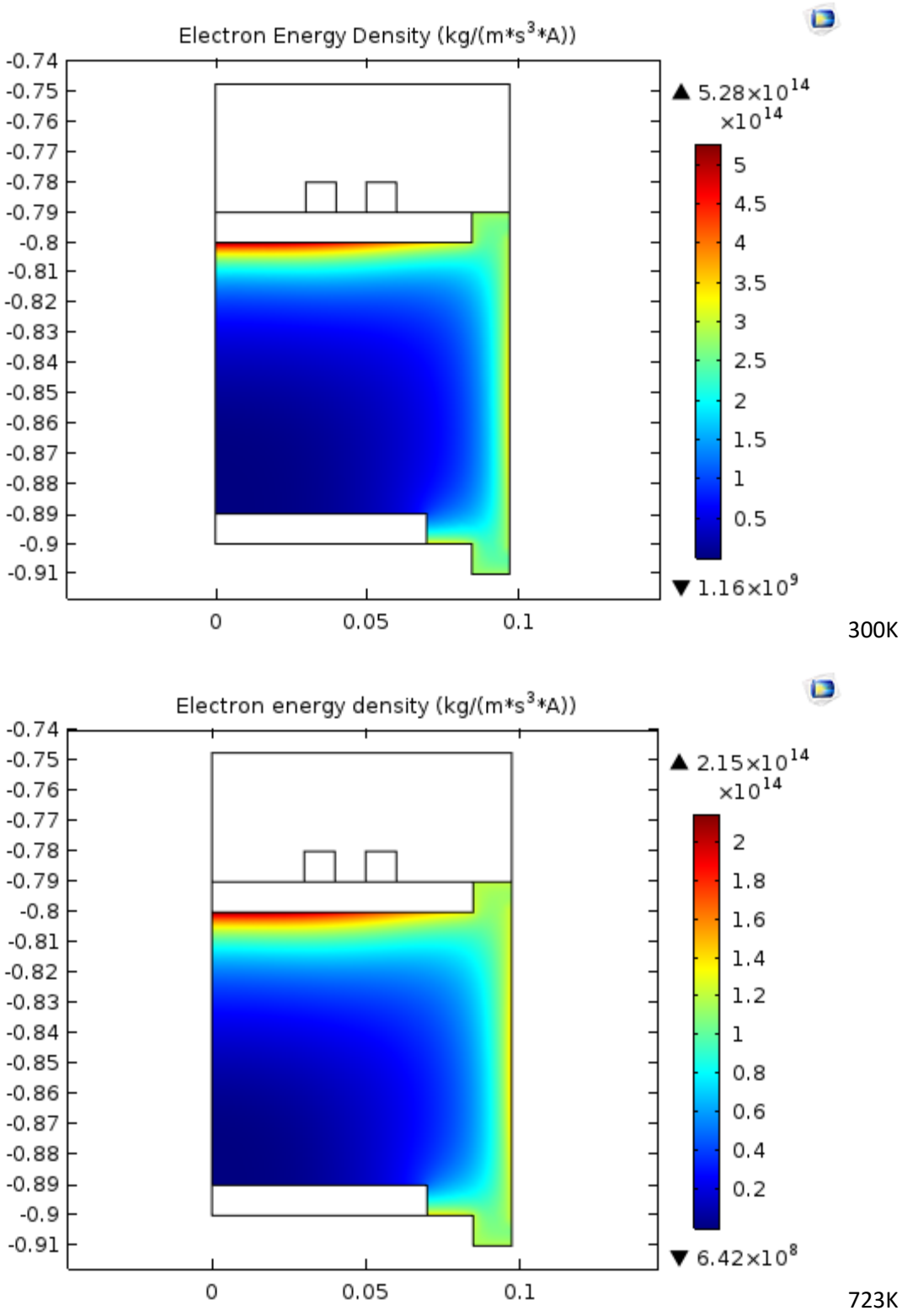

Fig 5.12: Shows electron energy densities at two different temperatures. Respective maximum values being (a) 5.28×10^{14} for 300K and (b) 2.15×10^{14} for 723K.

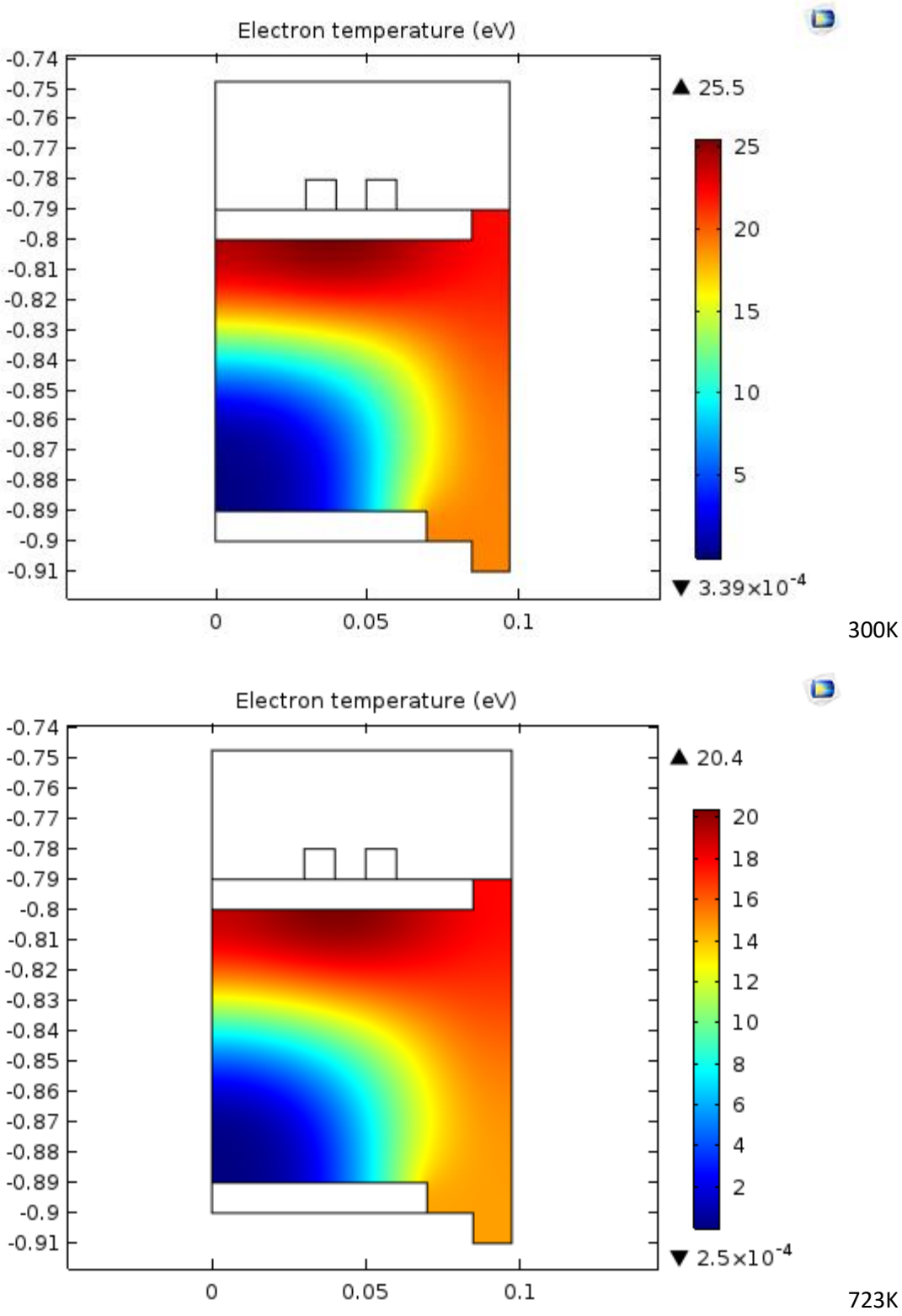

Fig 5.13: Shows electron temperature (eV) at two different gas temperatures. Respective maximum values being (a) 25.5 for 300K and (b) 20.4 for 723K.

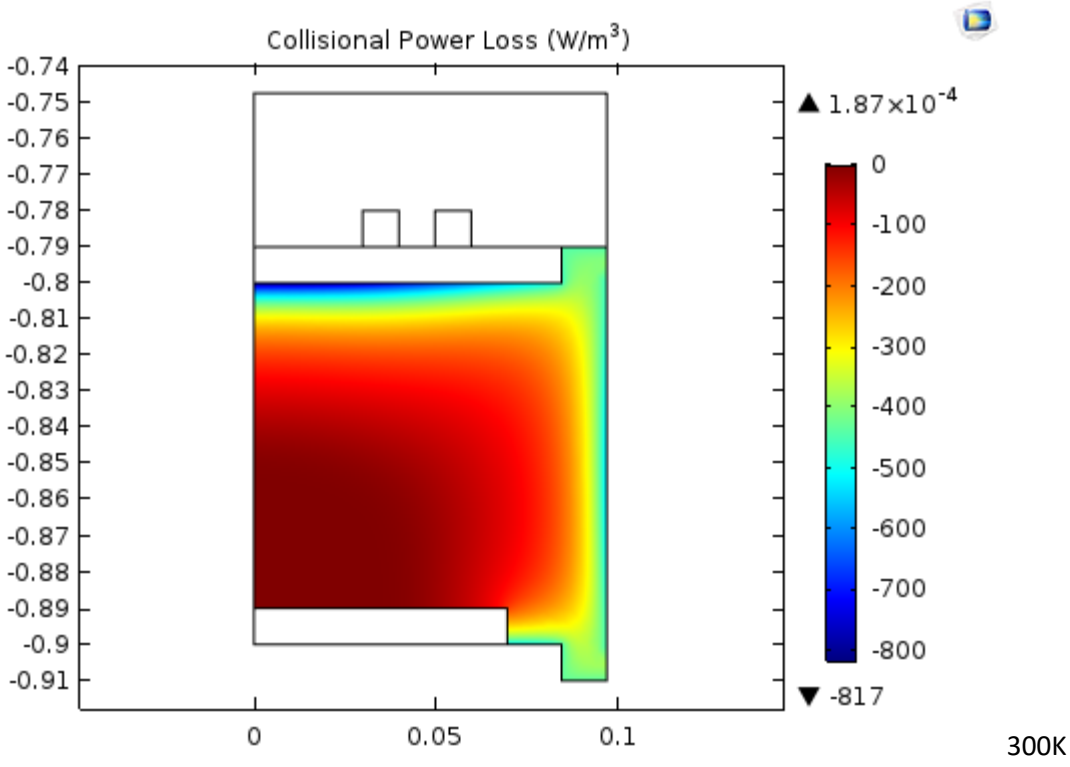

300K

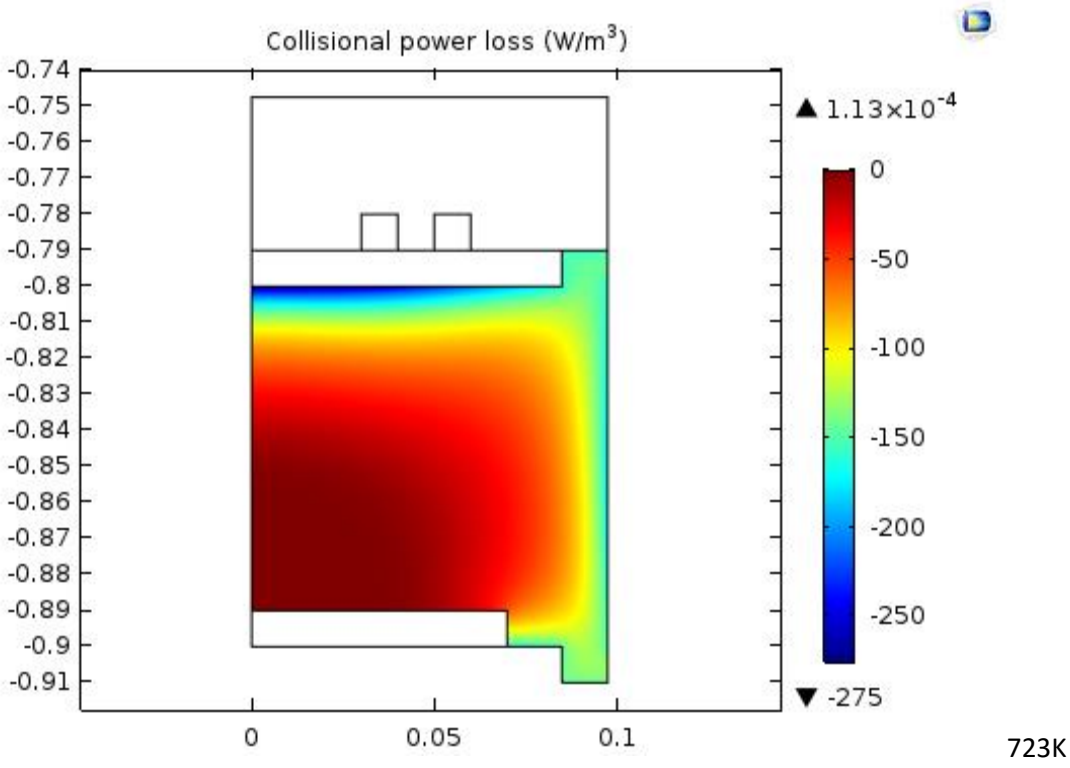

723K

Fig 5.14: Shows collisional power loss at two different temperatures. Respective maximum values being (a) 817 for 300K and (b) 275 for 723K.

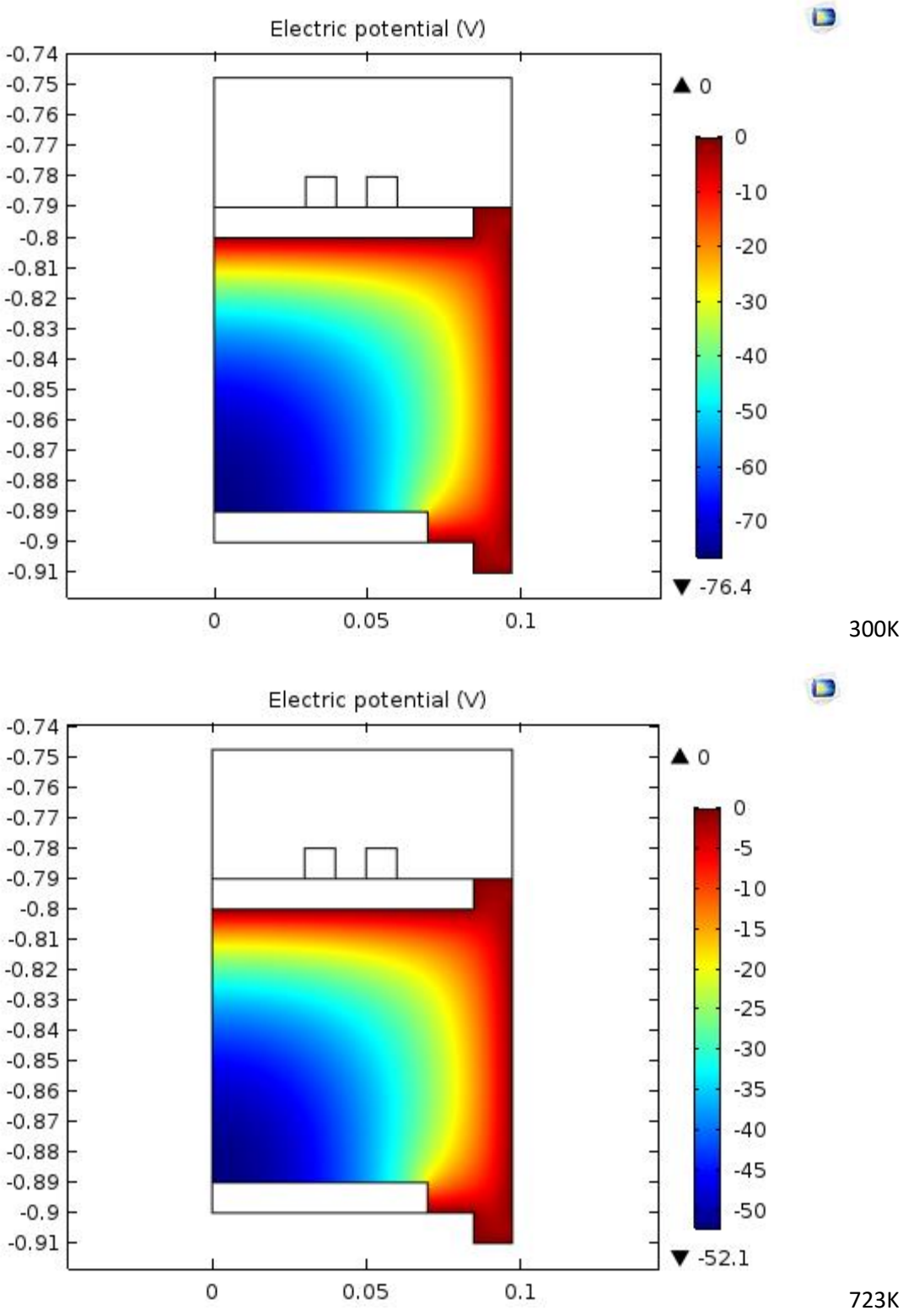

Fig 5.15: Shows electric potential (V) on the negative side at two different temperatures. Respective maximum values being (a) 76.4 for 300K and (b) 52.1 for 723K.

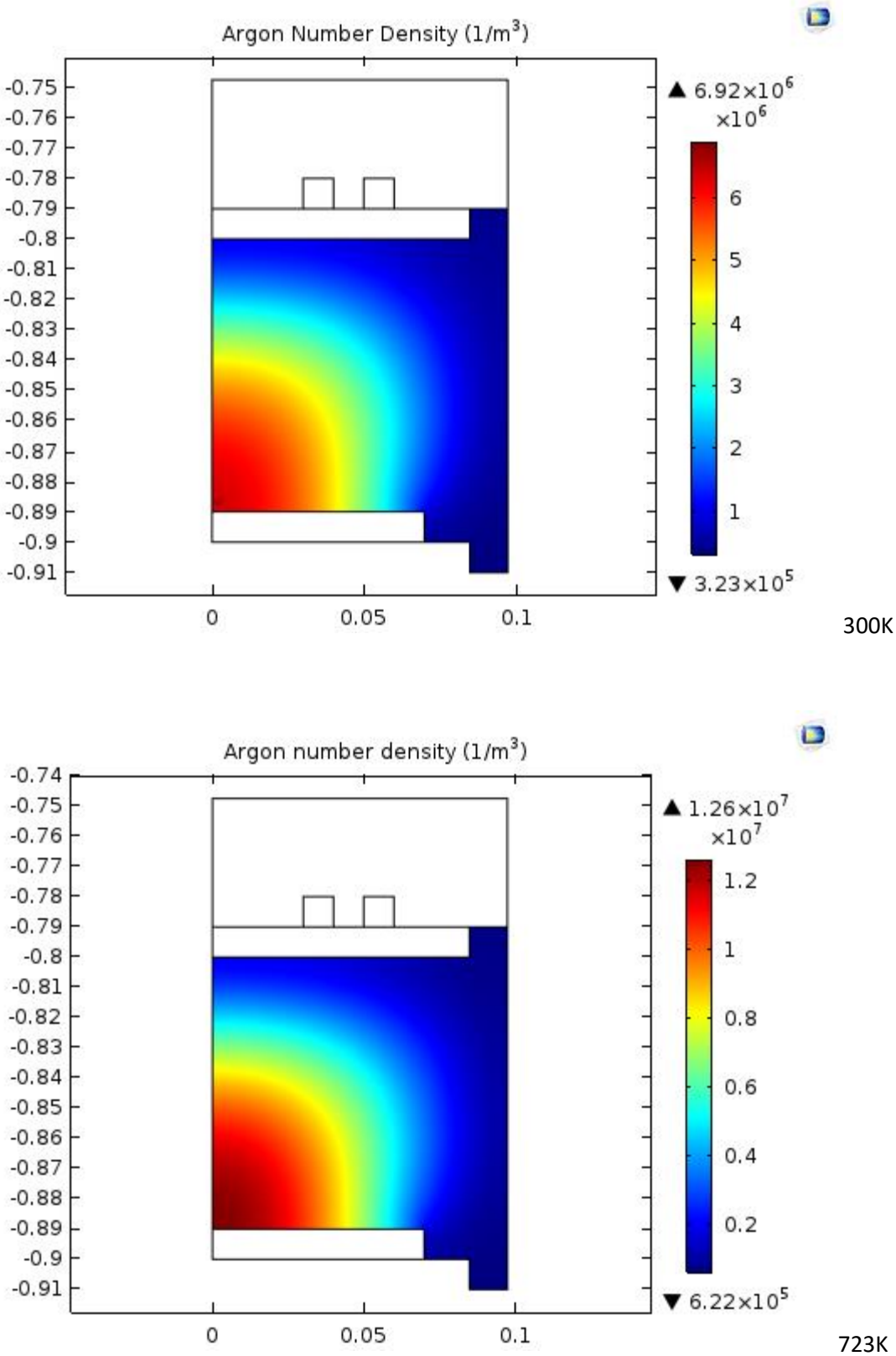

Fig 5.16: Shows Argon number densities at two different temperatures. Respective maximum values being (a) 6.92×10^6 for 300K and (b) 1.26×10^7 for 723K.

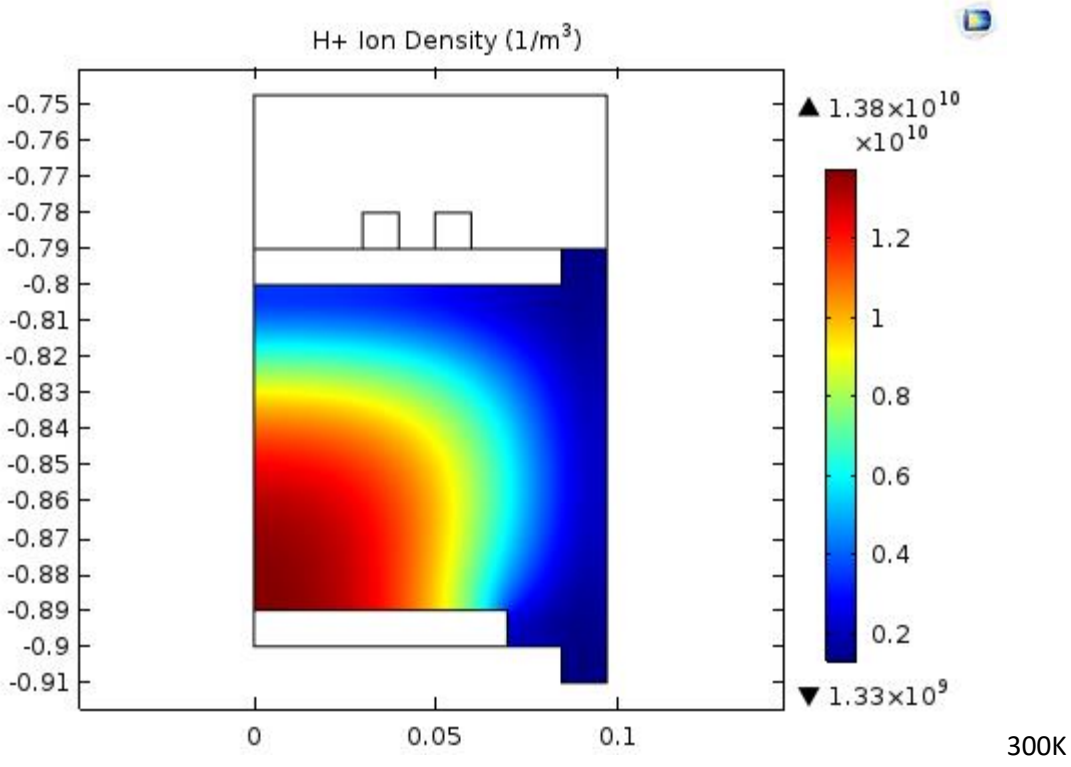

300K

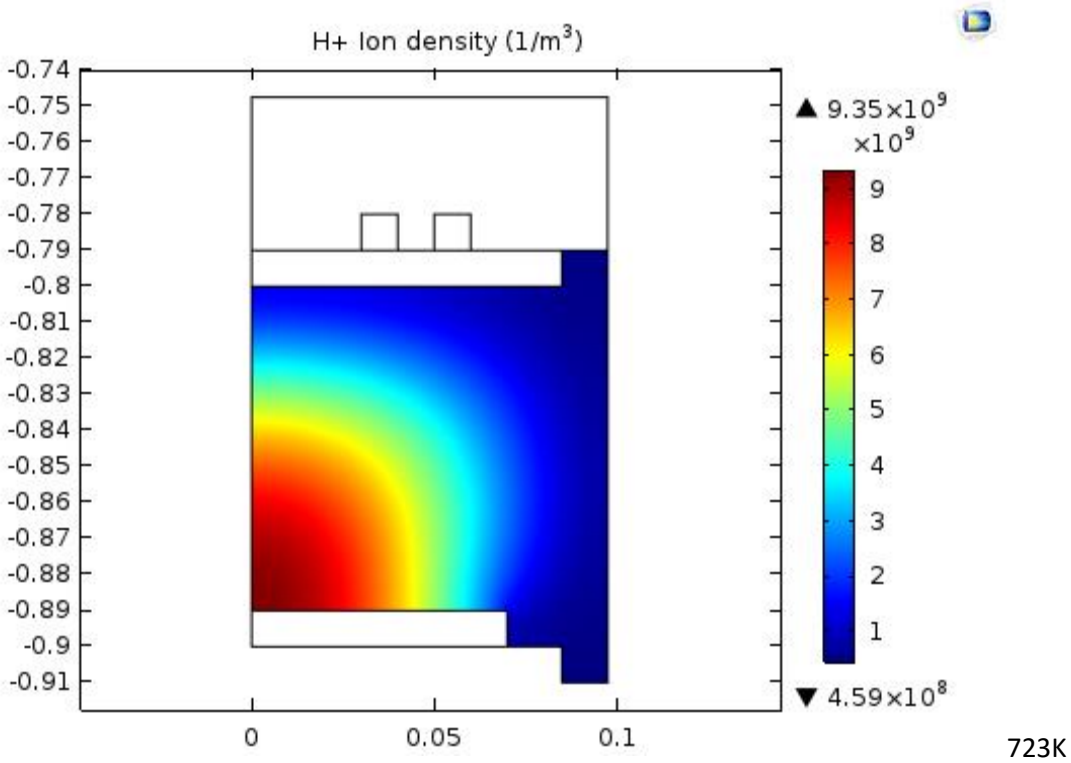

723K

Fig 5.17: Shows H+ ion densities at two different temperatures. Respective maximum values being (a) 1.38×10^{10} for 300K and (b) 9.35×10^{9} for 723K.

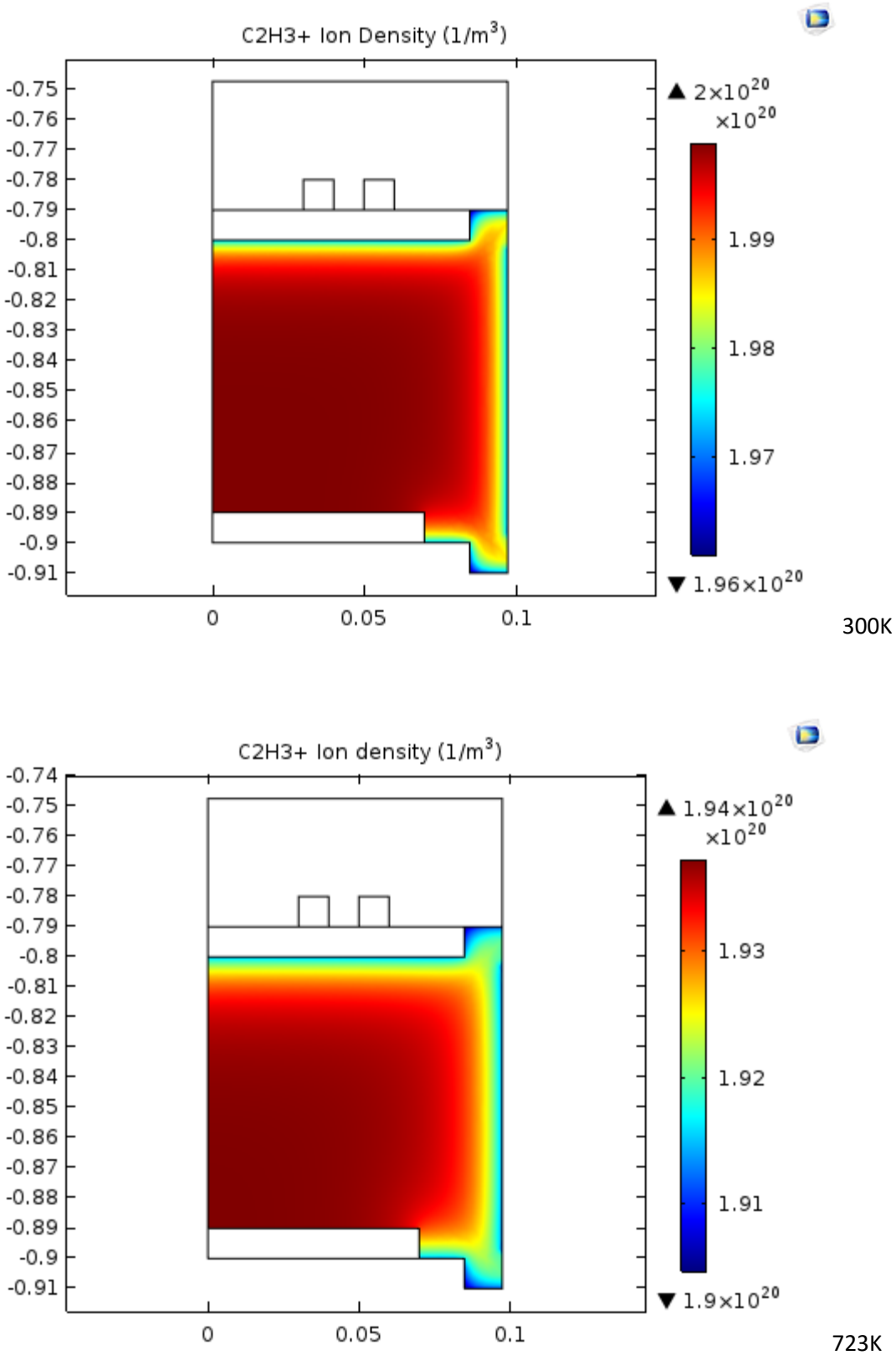

Fig 5.18: Shows C_2H_3+ ion densities at two different temperatures. Respective maximum values being (a) $2x10^{20}$ for 300K and (b) 1.94 $x10^{20}$ for 723K.

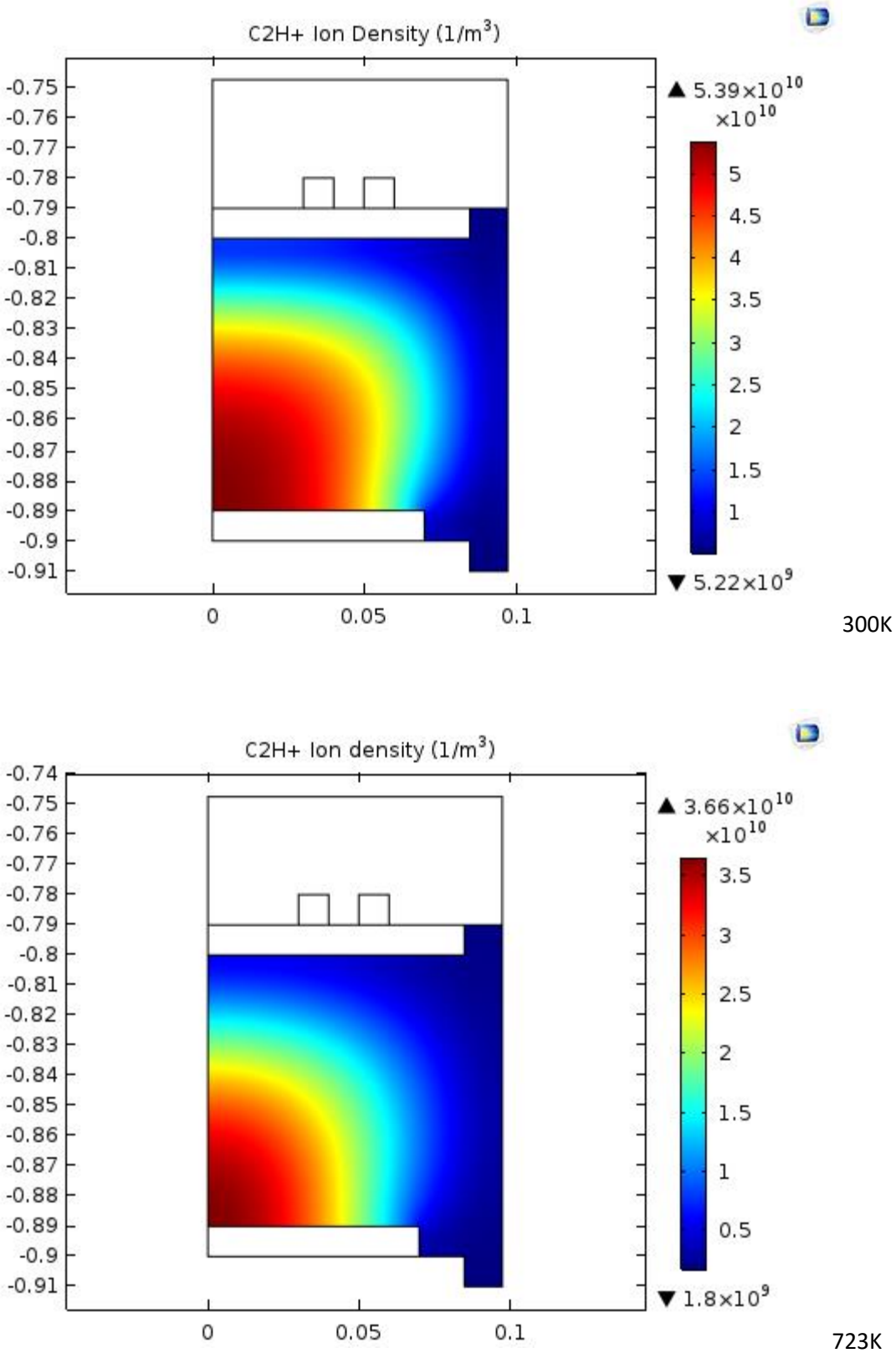

Fig 5.19: Shows C_2H+ ion densities at two different temperatures. Respective maximum values being (a) $5.39x10^{10}$ for 300K and (b) $3.66\ x10^{10}$ for 723K.

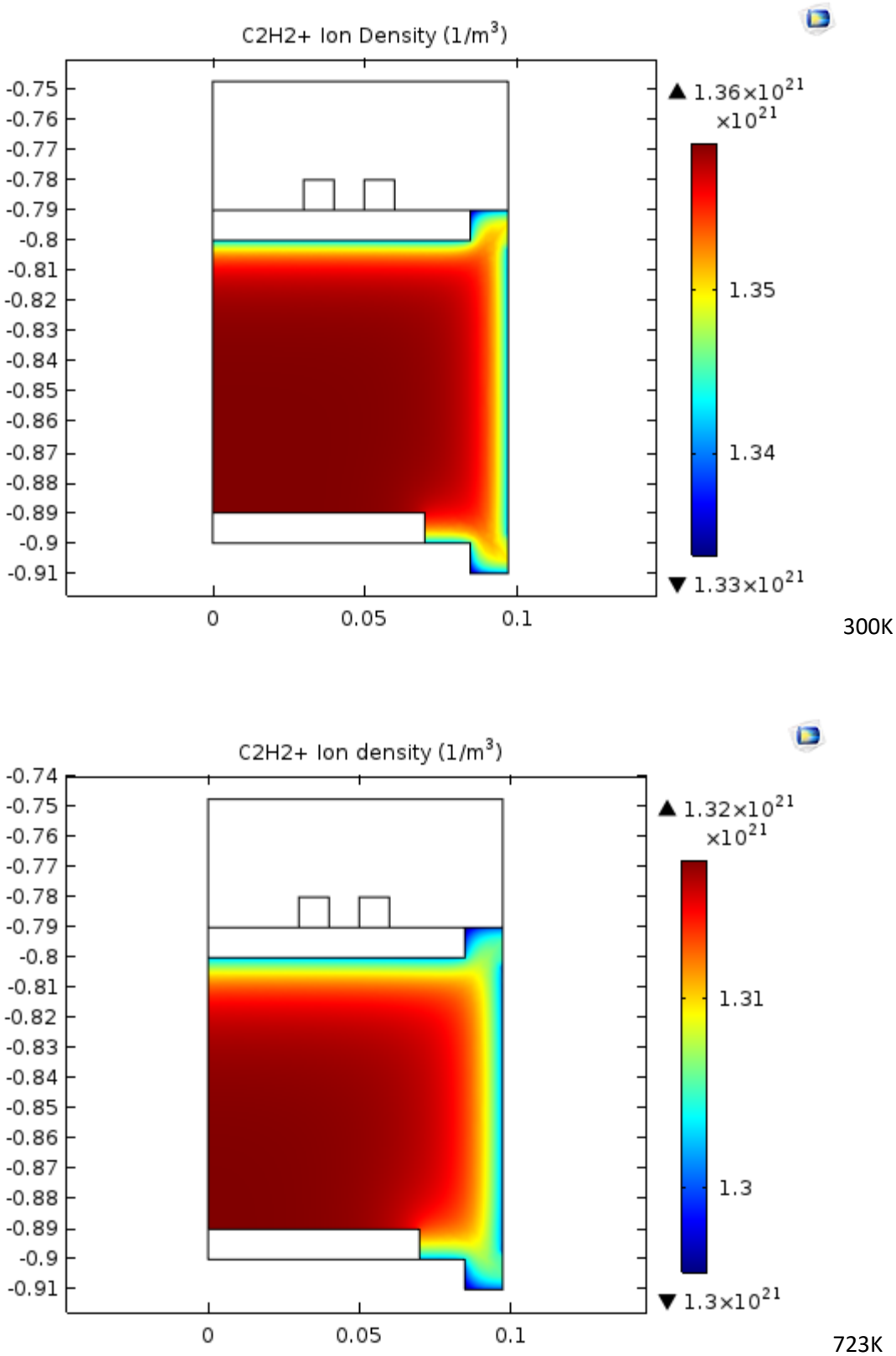

Fig 5.20: Shows C_2H_2+ ion densities at two different temperatures. Respective maximum values being (a) $1.36x10^{21}$ for 300K and (b) $1.32\ x10^{21}$ for 723K.

6

Future Aspects

Fullerenes and carbon nanostructures have demonstrated an extensive variety of one of a kind physical and substance properties that make them alluring for the production of new radical materials. Applications envelop a wide range of advancements and numerous improvements depend on new materials and our capacity to comprehend their properties. More research around there is unmistakably expected to completely investigate the conceivable outcomes offered by these materials, for instance, in nano science, biosensors, and photovoltaic. As the field is quickly changing, the recently framed fullerenes, nanotubes, and carbon nanostructures division is keen to be as comprehensive as would be prudent and to widen our points of view.

While logical advances in the utilization of nanotechnology to the nutrition trade have been advancing quickly, improvement of nanotechnology related with nanostructures is comparatively much slower. As the exploration in sustenance nanotechnology builds, it likewise raises open concerns about security of the results of nanotechnology for consumption by humans and its usage [32]. Along these lines, a far reaching appraisal of potential dangers to human well-being is fundamental before the nano nourishment items are financially accessible. In any case, there has been an absence of a general guideline that is particularly created for the wellbeing evaluation of nano materials in nourishment. EU regulation built up that any food element coming about because of nano-innovative applications must experience security evaluation before being affirmed for its utilization [34]. A few rules were additionally discharged as of late from the United States Food and Drug Administration, which are identified with the utilization of nanotechnology in nourishment [31]. Obviously, sooner rather than later more examinations and directions concerning the effects of these nano-materials on human and natural wellbeing should be led and built up to guarantee our nourishment security [33].

7

Conclusion

The low-temperature plasmas are omnipresent in semiconductor producing as exemplified by the standard utilization of drawing and PECVD procedures in the IC business and the substantial scale accomplishment of hardware or equipment makers. Different areas, for example, plasma based display screens, plasma disinfection of therapeutic gear and modern coatings are real examples of overcoming adversity for low-temperature plasmas. Normally the outcome is the accessibility of an extensive body of the literature, business hardware and diagnostic devices, modelling and simulation capacities and an immense learning base. The nanotechnology look into network has perceived the adaptability and exceptional favorable circumstances of different releases and embraced the strategy to develop nanostructured materials and to a constrained degree, for additional handling of these materials. As found in this audit, the vast majority of these endeavors are in their beginning stages, aside from maybe on account of PECVD of CNFs and nanotubes, which has been examined all the more widely. Initial results in each of the areas are inspiring and the anticipation is that the utility of low-temperature plasmas in nanomaterial arrangement will see a huge development [8]. To encourage and additionally fuel this development, future investigations must spotlight on understanding systems in PECVD processes, application-particular development and related issues, vast scale wafer handling issues, end-to-end manufacture of a gadget based on a plasma-developed material and related process advancement, and so forth. In a considerable lot of these cases, it is known that plasma and surface diagnostics and demonstrating and simulation can be to a great degree profitable. There is a broad plasma network with the right skill in these areas yet their cooperation up to this point is exceptionally constrained, as confirm by the absence of papers dedicated to diagnostics and demonstrating. This will change when applications and commercialization empowered by nano-materials start to emerge and the outstanding buzzword 'in the event that you manufacture it, they will come' will apply to the joint effort between the nanotechnology and customary low-temperature plasma communities also.

References

[1]. Plasma-Enhanced Chemical Vapor Deposition: Where we are and the Outlook for the Future, Yasaman Hamedani, Prathyushakrishna Macha, Timothy J. Bunning, Rajesh R. Naik and Milana C. Vasudev DOI: 10.5772/64654, August 31st 2016.

[2]. Vasudev MC, Anderson KD, Bunning TJ, Tsukruk VV, Naik RR. Exploration of plasma enhanced chemical vapor deposition as a method for thin-film fabrication with biological applications. ACS Applied Materials & Interfaces; 5(10): 3983-94 (2013).

[3]. Yague JL, Coclite AM, Petruczok C, Gleason KK. Chemical vapor deposition for solvent-free polymerization at surfaces. Macromolecular Chemistry and Physics; 214(3):302-12 (2013).

[4]. Eichfeld SM, Hossain L, Lin Y-C, Piasecki AF, Kupp B, Birdwell AG, et al. Highly scalable, atomically thin WSe2 grown via metal-organic chemical vapor deposition. ACS Nano; 9(2):2080-7 (2015).

[5]. Pierson HO. Handbook of Chemical Vapor Deposition [CVD]: Principles, Technology and applications. Park Ridge, NJ: Noyes Publication, 4, 114-118 (1992).

[6]. Stoffel A, Kovács A, Kronast W, Muller B. LPCVD against PECVD for micromechanical applications. Journal of Micromechanics and Micro-engineering; 6(1): 1 (1996).

[7]. Li X-L, Ge J-P, Li Y-D. Atmospheric pressure chemical vapor deposition: an alternative route to large-scale MoS2 and WS2 inorganic fullerene-like nanostructures and nano-flowers. Chemistry – A European Journal; 10(23): 6163-71 (2004).

[8]. M Meyyappan, Plasma nanotechnology: past, present and future, IOP Science, 5, 31-39, April 14 (2011).

[9]. Sheem, K.Y.; Song, E.H.; Lee, Y.H. High-rate charging performance using high-capacity carbon nanofilms coated on alumina nanoparticles for lithium-ion battery anode. Electrochim. Acta, 78, 223–228, (2012).

[10]. Yan Liang, beautifulchemistry.net/carbon-nanostructure.

[11]. S.O. Podgorny, I.P. Demeshko, O.T. Podgornaya, Cadmium telluride nanofilms application in carbon monoxide detection, IEEE, 28, 401-411 (2014).

[12]. Podgornyi S.O. , Podgornaya O.T. , Skutin E.D. , Demeshko I.P. Lukoyanova O.V, Fedotova K.I., Zinc selenide nanofilms application in carbon monoxide detection, 12, 121 (2016).

[13]. M. Meyyappan, L. Delzeit, A. Cassell, and D. Hash, Plasma Sources Sci. Technol. 12, 205 (2003), and references therein.

[14]. CNT technology overview, https://www.nanoscience.com/applications/education /overview/cnt-technology-overview/.
[15]. C. Bower, W. Zhu, S. Jin, and O. Zhou, Appl. Phys. Lett. 77, 830 (2000).
[16]. Changgu Lee, Xiaoding Wei1, Jeffrey W. Kysar , James Hone, Measurement of the Elastic Properties and Intrinsic Strength of Monolayer Graphene, Science, 321 (2008).
[17]. Taisuke Ohta, Aaron Bostwick, Thomas Seyller, Karsten Horn, Eli Rotenberg, Controlling the Electronic Structure of Bilayer Graphene, Science, 313 (2006).
[18]. Young-Woo Son, Marvin L. Cohen & Steven G. Louie, Half-metallic graphene Nanoribbons, Nature volume 444, pages 347–349 (2006).
[19]. Tsai, S.H., Chiang, F.K., Tsai, T.G., Shieu, F.S., and Shih, H.C. Synthesis and characterization of the aligned hydrogenated amorphous carbon nanotubes by electron cyclotron resonance excitation. Thin Solid Films, 366(1): 11–15. (2000).
[20]. Tomohiro Okumura. Inductively Coupled Plasma Sources and Applications. Physics Research International Volume, (2010).
[21]. T. Okumura and I. Nakayama, “New inductively coupled plasma source using a multi-spiral coil," Review of Scientific Instruments, vol. 66, no. 11, pp. 5262–5265, (1995).
[22]. T. G. Beuthe, J. S. Chang, Jpn. J. Appl. Phys., Part 1, 38, 4576, (1991).
[23]. A. Bogaerts, K. de Bleecker, V. Georgieva, I. Kolev, M. Madani, E. Neyts, Plasma Process. Polym, 3, 110 (2010).
[24]. UMIST, http://www.udfa.net/
[25]. I. Denysenko, N. A. Azarenkov, J. Phys, D: Appl. Phys., 44(174), 031 (2011).
[26]. I. Denysenko, K. Ostrikov, J. Phys. D Appl. Phys., 42, 015208, (2009).
[27]. Z. Marvi, S. Xu, G. Foroutan, K. Ostrikov, Phys. Plasmas, 22, 013504 (2015)
[28]. I. Denysenko, K. Ostrikov, Appl. Phys. Lett, 90(251), 501(2006).
[29]. H. Mehdipour, K. Ostrikov, A. E. Rider, Nanotechnology, 21(455), 605, 2010.
[30]. I. Denysenko, K. Ostrikov, M. Y. Yu, N. A. Azarenkov, J. Appl. Phys. 2007, 102, 074308, (2010).
[31]. Richard S. Myers. Collision theory, *J. Chem. Educ 55(4).*, (1978).
[32]. M. Gryziński. Theoretical description of collisions in plasma: classical methods. Journal de Physique Colloques, 40 (C7), (1979).
[33]. Francis D'Souza. Carbon bucky-balls to nanotubes; The Electrochemical Society Interface, Summer, 2, 15, (2006).
[34]. KavithaPathakoti[a] ManjunathManubolu[b] Huey-MinHwang[a] , Nanostructures: Current uses and future applications in food science, Journal of Food and Drug Analysis Volume 25, Issue 2, Pages 245-253, April 2017.